

Facultad de Física  
Departamento de Física Atómica, Molecular y Nuclear



VNIVERSITAT  
DE VALÈNCIA

# TRITIUM: Design, construction and commissioning of an in-water tritium detector

Marcos Martínez Roig

PhD in Physics

February 6, 2021

Under the supervision of:

José Díaz Medina

Nadia Yahlali Haddou



*Dedicated to  
my family*

Sometimes it's the people no one imagines anything  
of whom do the things that no one can imagine.

"Alan Turing"

I



# Acknowledgements

Al echar la mirada atrás a estos años de trabajo y formación como investigadora, siento que ha habido muchas personas que me han ayudado directa o indirectamente en esta aventura, por lo que no puede faltar este espacio para agradecer la ayuda que he recibido.

Durante estos 4 años han sido muchas las personas que me han ayudado. Espero no dejarme a nadie.

Ver memoria de "Detectores monolíticos y sensores compatibles con altos campos magnéticos para tomografía por emisión de positrones"

AGRADECER A:

- Gente de tritium Valencia: PEPE, NADIA, MIREIA, ANA, MARQUITOS, ANDREA.
- Gente del LARAM -> TERESA, VANESA, ROSA, CLODO
- Gente de Tritium -> GENTE DE PORTUGAL, Antonio y Jose Angel de extremadura, gente de francia...
- Gente que ha aportado al trabajo:
  - Gente de DUNE (Anselmo, Miguel, Justo)
  - Gente de NEXT (Vicente, Marc, Javier, la chica, etc...)

- Ingeniero electrónico David Calvo del IFIC
  - Gente del IFIMED (Ana Ros, Jhon Barrio y Gabriela Llosa del IFIMED, Rita, Jorge, Marina)
  - Gente de Espectrometría Gamma (El hombre y su mujer, Cesar, Ion, el doctorado, etc)
  - Gente de ATLAS (Urmila, Carlos Mariñas)
  - Gente del ICMOL (El que manda, Lidon)
  - Departamento de mecánica del IFIC (Manolo "Apellidos", Jose Luis Jordan, Jose Vicente Civera Navarrete, Tchogna Davis, Daniel)
  - departamento de electrónica del IFIC (Jorge Nacher Arándiga, Manu ... y el otro )
  - Al departamento de informática (gente)
- Gente externa que ha ayudado
    - DAVID CANAL DE SAMTEC
    - A LUIS FERR... DE PETSYS..
  - Gente externa que no ha ayudado
    - Grupo de amigos del IFIC (nombrar a todos, tanto en el master como en el doctorado)
    - Familia
    - Amigos del pueblo
  - Al programa interreg sudoe -> Soporte financiero!

# Abstract

Tritium is one of the most frequently emitted radioisotopes in a nuclear power plant. Large quantities of tritium are normally produced in the water of their cooling system, which are finally emitted to the environment. Due to the fact that high quantities of tritium could be dangerous for human health and for the environment, there exist several legislations around the world which try to control this radioactive emissions in each country, like the Directive Europeen 2013/51/Euratom, which establishes the tritium limit in drinking water in Europe at 100 Bq/L, or the U. S. Environmental Protection Agency, in United States, whose tritium limit in drinking water is established at 740 Bq/L.

Nowadays, due to such a low energy emitted in the tritium decay, we need high sensitive detectors for measuring it like LSC. The problem with LSC is that it is a off-line method whose measurement process can take up to 3 or 4 days, too much time if there are any problem with the NPP.

Detectors based on solid scintillators is a promissing idea for building a tritium detector that works in quasi-real time. This type of detectors has been developed so far succesfully but without achieving enough sensibility for measuring the legal limits.

In this study the results of TRITIUM project is presented. In the

## VI

framework of this project we have developed a quasi-real time monitor for low tritium activities in water. This monitor is based on a tritium detector that contains several detection cells which we read in parallel, several active vetos and a passive shielding for reduce the natural background of our system and an ultrapure water system to prepare the sample before we measure. Each detection cell is made up of hundreds of scintillating fibers read out by PMTs or SiPM arrays.

The final objective of this monitor will be the radiological protection around the nuclear power plant. This monitor will provide an alarm in case of an unexpected tritium release. It will be included in the early alarm system of Extremadura consisting of several detectors whose objective is to reduce the impact of Nuclear Power Plants to the environment.

**Keywords:** una, dos, tres...

# Nomenclature and Acronyms

Acronyms:

<i>OECD</i>	— Organisation for Economic Co-operation and Development
<i>UN</i>	— United Nations
<i>UNFCCC</i>	— The United Nations in the framework convention about Climate change
<i>ITER</i>	— International Thermonuclear Experimental Reactor
<i>NPP</i>	— Nuclear Power Plants
<i>DOE</i>	— Department of Energy
<i>U.S.A.</i>	— United States of America
<i>U.S.</i>	— United States
<i>EPA</i>	— Environmental Protection Agency
<i>LDL</i>	— Lower Detection Limit
<i>UDL</i>	— Upper Detection Limit
<i>PWR</i>	— Pressurized Water Reactor
<i>BWR</i>	— Boiled Water Reactor
<i>HWR</i>	— Heavy Water Reactor
<i>GCR</i>	— Gas-Cooled Reactor
<i>PHWR</i>	— Pressurized Heavy Water Reactor
<i>quasi-real</i>	— Less than 10 minutes
<i>LSC</i>	— Liquid Scintillation Counting
<i>LWR</i>	— Liquid Water Reactor
<i>IC</i>	— Ionization chamber

<i>BIXS</i>	— Beta Induced X-ray Spectrometry
<i>PMT</i>	— Photoelectron Multiplier Tube
<i>SDD</i>	— Silicon Drift Detector
<i>EEC</i>	— European Economical Community
<i>SiPM</i>	— Silicon Photoelectron Multiplier
<i>CNRS</i>	— Le Centre National de la Recherche Scientifique, France
<i>ALARA</i>	— As Low As Reasonably Achievable
<i>PMMA</i>	— Polymethyl Methacrylates
<i>CCD</i>	— Charge-Coupled device
<i>HV</i>	— High Voltage
<i>QE</i>	— Quantum Efficiency
<i>CE</i>	— Collection Efficiency
<i>SiPM</i>	— Silicon PhotoMultiplier
<i>APD</i>	— Avalanche Photodiode
<i>MPPC</i>	— Multi-Pixel Photon Counter
<i>G – APD</i>	— Geiger Avalanche Photodiode
<i>SSPM</i>	— Solid State PhotoMultiplier
<i>MRS – ADP</i>	— Metal-Resistor-Semiconductor Avalanche Photodiode
<i>MAPD</i>	— Micro-Pixel Avalanche Photodiode
$\lambda$	— wavelength
$\lambda_p$	— Wavelength at which we have the maximum of the associated spectrum
<i>PDE</i>	— Photodetection Efficiency of the SiPM
$C_t$	— Terminal capacitance of the SiPM
$G_{SiPM}$	— Gain of the SiPM
$V_{BR}$	— Breakdown voltage of the SiPM
$\Delta TV_{op}$	— Temperature coefficient ( $\text{mV}/^\circ\text{C}$ )
$q_e$	— Electron charge
$\sigma_T$	— Total uncertainty of the measurement
$\sigma_{st}$	— Stadistical component of the uncertainty
$\sigma_{si}$	— Sistematically component of the uncertainty
$A_m$	— Activity measured

## Atomic and nuclear symbols

$\text{CO}_2$	— Carbon Dioxide
$\text{CH}_4$	— Methane
$\text{N}_2\text{O}$	— Nitrous oxide
HFC	— Hydrofluorocarbons
PFC	— Perfluorocarbons
$\text{SF}_6$	— Sulfur Hexafluoride
${}^1_1\text{H}$	— Hydrogen
${}^2_1\text{H}$	— Deuterium (Non-radiactive hydrogen isotope, 1 neutron)
${}^3_1\text{H}$	— Tritium (radiactive hydrogen isotope, 2 neutrons)
${}^4_2\text{He}$	— Helium
${}^3_2\text{He}$	— Isotope of the Helium(Non-radiactive, 1 neutrons)
${}^{14}_7\text{N}$	— Nitrogen
${}^{12}_6\text{C}$	— Carbon
${}^6_3\text{Li}$	— Lithium isotope
${}^7_3\text{Li}$	— Lithium
${}^{10}_5\text{B}$	— Boron
${}^{16}_8\text{O}$	— Oxygen
${}^{222}_{86}\text{Rn}$	— Radon
${}^{40}_{19}\text{K}$	— Potassium
${}^{137}_{55}\text{Cs}$	— Cesium
n	— free neutron
$\text{H}_2\text{O}$	— Usual water
$\text{D}_2\text{O}$	— Heavy water
HDO	— Semi heavy water
$T_{1/2}$	— Half-life time of a radioactive element
$\beta$	— Beta decay
$\bar{\nu}_e$	— Electron antineutrino
$e^-$	— Electron

## X

$\gamma$	— Gamma
$p$	— Proton
$\alpha$	— Alpha (nucleus with two protons)
$\sigma_i$	— Cross section of the "i" process
$\eta_{det}$	— Intrinsic detector efficiency
$F_{sci}$	— Active surface of the plastic scintillator
$\varepsilon_{det}$	— Specific detector efficiency
$mip$	— minimum ionizing particle

Units:

$Btu$	— British thermal unit
$STP$	— Standard temperature ( $0^{\circ}\text{C} = 273\text{K}$ ) and pressure (1 atm)
W	— watt
h	— hour
g CO <sub>2</sub> /kWh	— grams of CO <sub>2</sub> per kilowatt hour
L	— Liter
Bq	— Becquerel, Nuclear decay number per second
Bq/L	— Becquerel per liter
$Ci$	— Curios
$Ci/L$	— Curios por litro
$yr$	— year
$\mu S/cm$	— MicroSivers per centimeter
$kcps$	— kilo counts per second
$pF$	— picoFarads
A	— Ampere (C/s).
C	— Coulomb.
V	— Voltage.
T	— Temperature ( $^{\circ}\text{C}$ ).
$Vol$	— Volume (m <sup>3</sup> ).

Añadir en un futuro:

- $D\&D$  — Decontamination and Decommissioning.
- $DWS$  — Drinking water standars
- $NA$  — Numerical Apertures



# Contents

<b>Acknowledgements</b>	<b>III</b>
<b>Abstract</b>	<b>V</b>
<b>Nomenclature and acronyms</b>	<b>VII</b>
<b>List of Figures</b>	<b>XX</b>
<b>List of Tables</b>	<b>XXII</b>
<b>1 Introduction</b>	<b>1</b>
1.1 Global energy context . . . . .	1
1.2 Tritium properties . . . . .	11
1.3 State-of-the-art in tritium detection . . . . .	17
1.4 Tritium project and Tritium monitor . . . . .	21
1.5 Work scheme . . . . .	26

<b>2 Design principles</b>	<b>27</b>
2.1 Detector system overview . . . . .	27
2.2 Tritium detector . . . . .	30
2.2.1 Interaction of particles with matter . . . . .	32
2.2.2 Scintillators plastic . . . . .	35
2.2.3 The light detection in photosensors . . . . .	44
2.2.4 Readout system of photosensors . . . . .	63
2.3 Ultrapure water system . . . . .	76
2.3.1 Introduction water system . . . . .	76
2.3.2 Set up water system . . . . .	77
2.4 Background rejection system . . . . .	80
2.4.1 Set up passive shield . . . . .	82
2.4.2 Set up Active veto . . . . .	84
<b>3 Research &amp; Development</b>	<b>89</b>
3.1 Introduction . . . . .	89
3.2 Characetrization fibers . . . . .	91
3.3 Characterization SiPM . . . . .	97
3.4 Characetrization water system . . . . .	100
3.5 Characterization shields . . . . .	101

3.5.1	Passive shield (lead) . . . . .	101
3.5.2	Active shield (cosmic veto) . . . . .	101
<b>4</b>	<b>Tritium monitor prototypes</b>	<b>103</b>
4.1	Preliminary prototypes . . . . .	103
4.1.1	Tritium-IFIC 0 . . . . .	103
4.1.2	Tritium-IFIC 1 . . . . .	103
4.1.3	Tritium-Aveiro . . . . .	103
4.2	Tritium-IFIC 2 . . . . .	104
4.3	Modular TRITIUM prototype . . . . .	105
<b>5</b>	<b>Simulations</b>	<b>107</b>
<b>6</b>	<b>Results and discussion</b>	<b>109</b>
6.1	Results from laboratory measurements . . . . .	109
6.2	Results in Arrocampo dam . . . . .	110
6.3	Results in simulations . . . . .	111
<b>7</b>	<b>Conclusions and prospects</b>	<b>113</b>
<b>Appendices</b>		
<b>A</b>	<b>Birks coefficient study</b>	<b>117</b>

B Signal processing in NIM modules	119
C Electronical schemes of PCBs used for SiPM characterization	121
D Ultrapure water system	123
Bibliography	127

# List of Figures

1.1	World energy consumption from 1990 up to now and outlooks for the future until 2040 (units in $10^{15} \text{ Btu}$ ) [2] . . . . .	2
1.2	Tritium decay . . . . .	13
1.3	Energy spectrum of tritium electrons [30] . . . . .	14
1.4	Arrocampo dam, Almaraz NPP and Tajus river . . . . .	23
2.1	Scheme of the scintillator detector [?] . . . . .	31
2.2	Domain regions of the three most probable types of interactions of gamma rays with matter. The lines show the values of $Z$ and $h\nu$ where the two neighboring effects are equally likely. [55] [56] . . . . .	33
2.3	Jablonsky diagram. [55] . . . . .	37
2.4	Stokes shift. [55] . . . . .	38
2.5	Emission spectrum of BCF-12 fibers of Saint-Gobain. [57] . .	41
2.6	How photons are collected in a fiber with single clad. [57] . .	42

2.7 Scheme of a PMT. [55] . . . . .	45
2.8 Quantum efficiency spectrum for the PMT used (R8520-ZB277). [62]	47
2.9 Hamamatsu commercial voltage divider electronic circuit. Upper circuit with negative supply and lower circuit with positive supply. [62] . . . . .	48
2.10 Energy band scheme for (a) insulator, (b) semiconductor and (c) conductor. [56] . . . . .	51
2.11 Crystal lattice and energy band scheme formed by a silicon with (left) a pentavalent dopant that creates an n-type semiconductor (right) a trivalent dopant that creates a p-type semiconductor. [56] . . . . .	53
2.12 (Above) Schematic of the charge distribution and electric field created in a pn-junction. (Bottom) Commonly used symbol for a diode. [63] . . . . .	53
2.13 Scheme of a APD and electrical symbol used. [64] . . . . .	56
2.14 Using persistence on the oscilloscope to show several pulses with different heights. Each height associated with a different number of SiPM pixels lit at the same time. . . . .	57
2.15 (Left) Electronic scheme of a SiPM and (right) output current of a SiPM as a function of the reverse voltage. It show that the quenching mechanism is essential for working with SiPMs [69] . . . . .	58
2.16 Schemes of different electronic configuration used to measure with PMT. . . . .	66

2.17 Different situation that can happen when we do time coincidences with PMTs. . . . .	70
2.18 Signal amplified and logical gate (input signals of MCA). . . . .	71
2.19 Energy spectrum obtained with the electronic configuration explained in this section for four PMTs. . . . .	71
2.20 Different parts of PETSYS system. [82] . . . . .	72
2.21 Three PCBs used for the SiPM characterization and LED emission spectrum. . . . .	75
2.22 Scheme of water purification system. . . . .	78
2.23 Lead Bricks and their arrangement in the lead shielding. . . . .	83
2.24 Lead Bricks and their arrangement in the lead shielding. . . . .	83
2.25 Active veto and Tritium-IFIC 2 prototype in an aluminum mechanical structure developed by IFIC's mechanical engineering department. . . . .	85
2.26 Hard cosmic events detected with the active veto of TRI-TIUM: a) Affecting to the tritium measurement, b) Does not affecting to the tritium measurement. c) Hard cosmic muon rate. . . . .	86
2.27 Emission energy spectrum of the plastic scintillation used for the active vetos. [90] . . . . .	88
2.28 Different layers used to cover of the active veto. . . . .	88
3.1 Unsuccessful results of using commercial techniques to cut fibers. . . . .	93

3.2	Microscopes used to check the results. . . . .	93
3.3	Cutting device developed in the TRITIUM experiment and additional part to make precise measurements of fiber length. . . . .	94
3.4	Result of the polishing process. a) Fiber end after cutting with TRITIUM devices b) Fiber end after cutting with TRITIUM devices and polishing with Thorlabs technic. . . . .	96
D.1	Scheme of the ultrapure water system. . . . .	123
D.2	Different stages of filtration of the ultrapure water system. . . . .	124
D.3	Doble phase reverse osmosis stage and containers used to store the outlet water of the ultrapure water system. . . . .	125
D.4	Siemens PLC, software for remote control of ultrapure water system. . . . .	125
D.5	General photo of the complete ultrapure water system. . . . .	126
D.6	Raw water, reject water and ultrapure water obtained with this system. . . . .	126

# List of Tables

1.1	Fusion reactions between deuterium and tritium[6] . . . . .	3
1.2	Estimations of CO <sub>2</sub> emissions for several kinds of energy sources[8] . . . . .	5
1.3	Contribution of each energy source to the total energy consumed in Spain in 2019 [9] . . . . .	5
1.4	Emission of tritium in different types of nuclear reactors[16]	8
1.5	Mean Free Path of tritium isotope for several energies and several environments [25] . . . . .	15
1.6	Gas molecules of hydrogen isotopes and their boiling points .	16
1.7	State-of-the-art in the tritium detection for different techniques [30] . . . . .	17
1.8	Results of different scintillator detector for tritium detection [30] . . . . .	20
2.1	Critical angles associated to different interfaces created with polystyrene, $n_0 = 1.6$ , and other materials . . . . .	43



# Chapter 1

## Introduction

### 1.1 Global energy context

The energy necessities around the world has been increased a 60% in the last 25 years and they are growing each day due to, mainly, the strong population growth (mundial population has been increased in a 40% between 1990 and 2015) and the fast development of emerging countries like China, India and Brazil. [1].

On top of that the outlook is that these energy necessities will keep increasing as you can see in the figure 1.1a, specially for countries which don't belong to the OECD like countries which I have said before. In this figure you can see that the energy quantity which will be used on 2040 is expected to be the double of the one which we used in 2000.

Nowadays, as you can see in the figure 1.1b, the most used elements for getting the energy that we use are liquid fuels, coal and natural gas, namely, natural elements. This fact has two problems. On the one hand, natural elements are limitated and this is a problem due to the huge

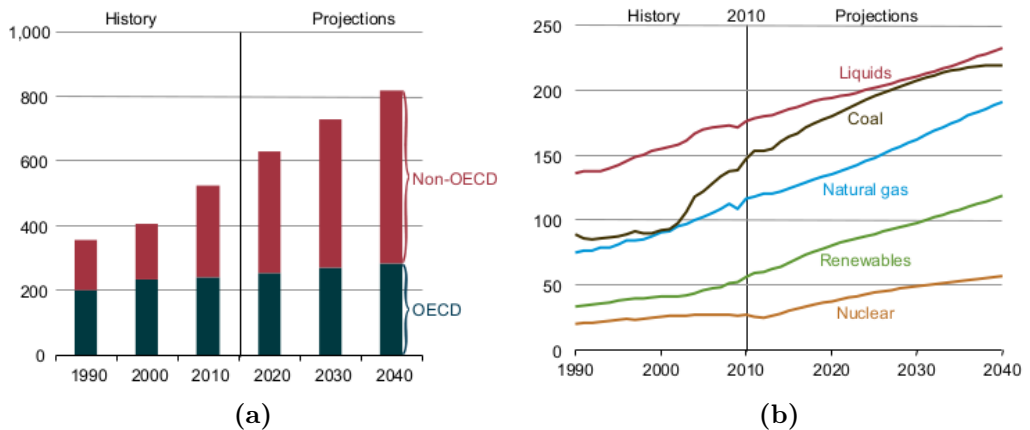


**Figura 1.1** – World energy consumption from 1990 up to now and outlooks for the future until 2040 (units in  $10^{15} \text{ Btu}$ ) [2]

increasing of the energy consumed in the world and, on the other hand, obtaining energy from these natural elements produces large amounts of greenhouses gases (mainly  $\text{CO}_2$ ) which contribute to the environmental contamination, global warming, deforestation, etc. and this is a very big problem, specially right now, since United Nations (UN) did a communication on November 25, 2019 [3], where they claimed that the lifestyle of the world population has not changed in the last years and, as a reason of that, we achieved the highest level of the  $\text{CO}_2$  in the history.

In order to control these emissions, the United Nations in the Framework Convention about Climate Change (UNFCCC), has developed a protocol, whose name is Kyoto [4]. The objective of this protocol is to control and reduce the global negative environmental impact. It is focused on 6 different gases, carbon dioxide ( $\text{CO}_2$ ), methane ( $\text{CH}_4$ ), nitrous oxide ( $\text{N}_2\text{O}$ ) and other three types of fluorinate industrial gases (HFCs, PFCs and  $\text{SF}_6$ ), which are related with the greenhouse effect and whose consequence is the global warming. This convention only encourage to belonging countries to the United Nations to reduce their greenhouses gases emissions but this protocol commits the countries who has signed it to do so.

Therefore, we currently have a problem because, on the one hand, we want to maintain, even increase, this economic growth and for that we need to produce as much energy as we can but, on the other hand, we need to reduce the negative environmental impact. Hence, what we need is a energy source with which we can get a big quantity of energy with a very low greenhouse gases emisions. One possibility which we have is the nuclear fusion plants. They don't emit greenhouse gases and with its energy, which is practically limitless, we could satisfy the humanity's energy necessities .

The largest representative in this sector is the ITER [5] (International Thermonuclear Experimental Reactor) that is going to be the largest fusion reactor in the world. The ITER is currently under construction in Cadarache, France, and its objective is to provide the concept of sustained fusion. The nuclear reaction which ITER try to reproduce in the earth is the one that uses deuterium ( $^2_1\text{H}$ ) and/or tritium ( $^3_1\text{H}$ ) because it is the only one whose requirements of temperature (several hundreds of millions degrees) and pressure we can fulfill in the earth. Among the possible combinations between both (table 1.1), the choice of ITER is the nuclear reaction between deuterium and tritium in a 50:50 mixture because, as you can see in this table, it is the nuclear reaction with which we get the highest energy release.

Reaction	Products	Energy gain (MeV)
$^2\text{H} + ^3\text{H}$	$^4\text{He} + \text{n}$	17.6
$^3\text{H} + ^3\text{H}$	$^4\text{He} + 2\text{n}$	11.3
$^2\text{H} + ^2\text{H}$	$^3\text{H} + ^1\text{H}$	3.98
$^2\text{H} + ^2\text{H}$	$^3\text{He} + \text{n}$	3.25

Table 1.1: Fusion reactions between deuterium and tritium[6]

Nevertheles, the fusion power plants is not already prepared for working, they are still in experimental phase and its researchers need to solve some important problems like inestabilitiy vortex, materials which

withstand such high temperatures, etc. [7]. Hence, although we know that the nuclear fusion plants will be the energy of the future, nowadays, we have to wait until all their problems has been resolved.

Other possible energy source is the existing Nuclear Power Plants (NPPs). With the NPPs we can practically avoid the problem of the greenhouse gases emission. We have to take into account that, although the nuclear fission reaction doesn't emit greenhouse gasses, the total process to obtain the energy, which involves the uranium mining and milling, transport, uranium enrichment, etc., has a small contribution to the annual release of greenhouses gases. These emissions are difficult to estimate because, on the one hand, they depend on the NPP that we consider (for instance, there are studies which show that asian NPPs has higher emissions [8]) and, on the other hand, there are some tasks whose greenhouse gases emission are difficult to quantify[8].

There's exist a study [8] which analyzes 19 different studies of different NPPs. His estimation for the total greenhouses gases emision of a NPP is 66 g CO<sub>2</sub>/kWh which was obtained as a average of these 19 studies considered. In the table 1.2 this estimation is compared with the estimation for other energy kinds. There you can check that, the emissions due to NPPs is much more smaller, one order or more, than the emissions from burning natural elements.

NPPs are already working and, nowadays, they are essential for providing a big part of the electric power that is used in the current world (more than a 20% in Spain as you can see in the table 1.3).

NPP is one of the cheapest source. It is a stable source which doesn't depend on meteorological parameters and, although there are other alternative energy sources which are being developed quickly (photovoltaic, wind, tidal energy, etc.), even other concepts of energy production and saving (local production, solar roofs, energy efficiency, smart cities, etc.),

Technology	Estimate (g CO <sub>2</sub> /kWh)
Wind	9 – 10
Hydroelectric	10 – 13
Biogas	11
Solar thermal	13
Biomass	14 – 41
Solar PV	32
Geothermal	38
Nuclear	66
Natural gas	443
Fuel cell	664
Diesel	778
Heavy oil	778
Coal	960 – 1050

Table 1.2: Estimations of CO<sub>2</sub> emissions for several kinds of energy sources[8]

Type of energy source	Contr.	Type of energy source	Contr.
Nuclear	22.0%	Wind	20.9%
Coal	4.2%	Hydraulics	9.7%
Combined Cycle	20.1%	Solar Photovoltaic	3.5%
Cogeneration	11.8%	Solar thermal	2.0%
No-renewable waste	0.8%	Other renewables	1.4%
Pumping turbine	0.6%	renewable waste	0.3%
		Imported balance of international exchanges	2.7%

Table 1.3: Contribution of each energy source to the total energy consumed in Spain in 2019 [9]

today they are not develop enough to fully supply ourselves with them.

The detractors of nuclear energy argue that NPPs facilitate nuclear proliferation or there are a risk of radioactive contamination and accidents like it happened in the past: Chernobyl, Fukushima and other accidents with lesser impact such as Three Mile Island, near to Pensilvania, USA [10].

Although we know that the nuclear energy is not the energy of the future since it produces nuclear waste which, by the moment, we don't know how we can eliminate, it is difficult that we leave to use nuclear energy because, now, we don't have a better solution for obtaining the energy which we need.

In Spain the government are doing an effort in order to remove all nuclear power plants since they are not going to build new nuclear reactors and they are only waiting until the NPPs have reached the end of their useful life (approximately 40 years). They expect to close all NPPs between 2020 and 2030 [11].

Other countries like France, where the 77% of their energy consumed is obtained from nuclear sources, prefer to maintain their nuclear facilities and there's even exist other countries that believe that nuclear energy is a safe investment like China who announced in 2016 that they were going to build 60 new nuclear reactors in the next decade [12] or USA, who made an investment of 35 million of euros in 2019 for development and improvement of nuclear power plants [13].

In any case it is not important if we agree or not with nuclear energy source. The only important thing is that the nuclear energy production in the world is not going to stop in the next decade, in fact, it will increase as you have seen in the outlooks of the figure 1.1b. Therefore the development of different types of alarm systems is a good investment of both, time and money. Safety is not a negotiable aspect and there must

be mechanisms that warn us of any malfunction of a nuclear power plant. Hence, our work has based on the development of a monitor that we can use as early alarm in case of any problem happen in a NPP.

Generally, a nuclear reactor, which is working in normal mode, is characterized by extreme stability and, therefore, by a constant emission of radioactive isotopes so the first alarm signs of any malfunctioning of a NPP is a variation of this radioactive emission rate.

Between all the radioactive elements which is produced in a nuclear power plant, the most frequently produced is tritium as DOE complex [14] [15] and other research facilities in China [16] have seen in their installations and in ground water, surface water, and process waste water around their facilities. However, as we will see in the section 1.3, the current methods which is used for monitoring this radioactive element has some limitations.

For these reasons, the radioactive element which we have chosen for monitoring with our early alarm system is tritium. We have focused our alarm system for working with NPPs but it could be also interesting for other tasks where tritium is involved like monitoring the behaviour of future fusion nuclear plants (ITER will need up to several tens of kilograms of tritium for working, which correspond to several TBq of tritium) or any nuclear research facility (tritium is a common emission of these places [17],[18]), tracking the movement of tritium contaminated plumes in ground water [19] or demonstrate the compliance with the government agencies which fix the limit of the emitted radionuclides to the environmental.

We have to take into account that the limit of the emission of each radioactive element depends on the government agency who manages it, and the regulation directives that is implemented in that place so, as a consequence, it is different in each country. For example, in Europe, the agency that manages these limits is Council Directive and the limit which they have established for tritium in drinking water is  $A = 100 \text{ Bq/L}$  [20]. In

USA, the organization is United States Environmental Protection Agency (U. S. EPA) and this limit is  $A = 20 \text{ nCi/L} = 740 \text{ Bq/L}$  [21].

Tritium is normally produced in the water that there are in the cooling system or the moderator of some NPPs. It usually appear by neutron capture of the deuterium, which exist in the heavy water ( $D_2O$ ), semi-heavy water ( $HDO$ ) or the deuterium which has created by neutron capture in usual water ( $H_2O$ ). All these processes have a big probability to happen due to the huge quantity of neutrons which we has in the nuclear reactor,  $10^{14} \text{ n cm}^{-2}\text{s}^{-1}$  [22].

The quantity of tritium will be different for each reactor type because, as we will see in the next section, the cross section of tritium production will depend on the materials which there are in any type of NPP. In the table 1.4 we can see the emissions of different types of nuclear reactors:

Reactor type	Gaseous discharge (GBq/y)	Liquid discharge (GBq/y)
PWR	$3.70 \cdot 10^3$	$2.59 \cdot 10^4$
BWR	$1.85 \cdot 10^3$	$3.70 \cdot 10^3$
HWR	$7.40 \cdot 10^5$	$1.85 \cdot 10^5$
GCR	$7.40 \cdot 10^3$	$1.11 \cdot 10^4$

Table 1.4: Emission of tritium in different types of nuclear reactors[16]

The tritium which is created in the water of the cooling system is finally released partially or totally to the environment. Between these types, the most common way is HTO [16].

Our alarm system will monitor the activity of tritium in the water of the cooling system of the NPP which is emitted to the environmental. It can also work for the water of the moderator in these types of NPP but it's not our objective because it's a close circuit so it's not a emission (unless the moderator is leaking, in which case our alarm system would detect it indirectly due to a variation of tritium activity in the water of the cooling

system released to the environment).

The measurement of the tritium activity is one of the systematic environmental control which is performed during energy production by NPPs. It is normally done by LSC technic which has a very good detection capability and precision but it has some problems, for example, it needs too long time for taking a measurement (2 days or more). I will speak more about LSC technic in the section 1.3.

The detection of this tritium in quasi-real time ( $< 10$  min) is important because of the following reasons:

1. It can warn us about the production of an excessive number of neutrons in the nuclear reactor due to the overheating of itself or a leakage of the water from the primary circuit of the cooling system in a nuclear power plant due to some break (perhaps because of an excessive pressure, other alarm sign of a malfunctioning of a nuclear reactor). Both causes could become in a very dangerous problems so the tritium detection in quasi-real time could be important in order to quickly detect and to solve it.
2. The water, which there are in the secondary circuit of the cooling system, will be released to the environmental, usually rivers or seas, after using it for cooling purposes. Generally this water will be used later for human consuming, irrigation of all kind of plantations or it will arrive to a places where we fish.

Due to such a low legal limit in comparation with the activities of tritium inside of a nuclear reactor, it is possible that, if the nuclear power plant don't work correctly, the activity of tritium water released exceeds this limit and it become this water in no drinkable and these crops into inedibles. On top of that, the life time of tritium is more than 12 years so these places will remain contaminated during a lot of time.

3. There's exist a lot of rivers or seas, which is used for cooling systems of the nuclear power plants, that are crossborders, that's, they are shared by several countries like our case as we will see in the section 1.4. The emisión of an excessive tritium activity of one country could be affect severely to the other country creating new international conflicts between them.

Because of all these reasons it is very important that we have an alarm system which is capable of measuring such low tritium activities in quasi-real time. Nevertheless, as we will see in the section 1.3, currently there are not any technic with which we can fulfill these requeriments.

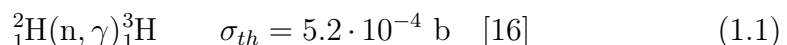
All these reasons has motivated the *Tritium* project, whose objective is the development of a system for quasi-real time monitoring of low radioactive levels of tritium in water for security applications in nuclear power plants.

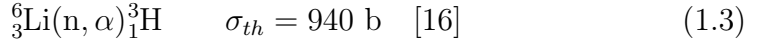
## 1.2 Tritium properties

Tritium is the only radioactive isotope of hydrogen. It was first time produced in 1934 from neutron capture of deuterium by Ernest Rutherford, Mark Oliphant and Paul Harteck [23] and it was first time isolated in 1939 by Luis Walter Alvarez and Robert Cornog [24], who checked that tritium is a radioactive element.

Tritium can be found in the environment since it is normally produced through the interaction of cosmic rays and gaseous elements of the upper atmosphere like nitrogen ( $^{14}\text{N}(\text{n}, ^3\text{H})^{12}\text{C}$ ) [25] and oxygen ( $^{16}\text{O}(\text{n}, ^3\text{H})^{14}\text{N}$ ) [26]. Then tritium becomes water (HTO) and reaches the earth's surface as rain with an estimated production rate of  $4 \cdot 10^6 \text{ Ci/yr}$  ( $1.48 \cdot 10^8 \text{ GBq/yr}$ ) [16] [25].

Tritium can be produced artificially in the environment from many different anthropogenic origins. There are a big amount of tritium which was produced on military nuclear test explosions between 1945 and 1975, whose estimated production rate is  $8 \cdot 10^9 \text{ Ci}$  ( $2.96 \cdot 10^{11} \text{ GBq}$ ) and a part of that still remains. It was mainly produced from the nuclear reactions  $^{14}\text{N}(\text{n}, ^3\text{H})^{12}\text{C}$  and  $^2\text{H}(\text{n}, \gamma)^3\text{H}$ . Tritium can be also produced by commercial producers of radioluminescent and neutron generator devices ( $1 \cdot 10^6 \text{ Ci/yr}$ ), nuclear power and defense industries (less than  $2 \cdot 10^6 \text{ Ci/yr}$ ), several research facilities and nuclear reactor operation ( $2 \cdot 10^6 \text{ Ci/GWyr}$ ), whose main production channels are [16] [25]:





Tritium is a radioactive element whose half-life time is  $T_{1/2} = 12.32$  years. It has one proton and two neutrons and decays exclusively through  $\beta^-$  radiation, that's, it doesn't have other type of radioactive decay. In this decay, one neutron of tritium is transformed in a proton plus electron and electron-antineutrino according to the following equation:



Then the nucleus of the tritium son has two protons and one neutron so it is a helium isotope,  ${}^3_2\text{He}$  which is stable. Therefore, the nuclear reaction which descript the  $\beta^-$  decay of the tritium is:



In the Figure 1.2 we can see the scheme of tritium energy levels. In this decay we practically don't have the possibility of detecting the neutrinos because it interacts very weakly with matter and, therefore, with our detector ( $\sigma \propto 10^{-42} \text{ cm}^2$  [27]) and, since  ${}^3\text{He}$  has a much larger mass than electrons and neutrinos, by conservation of energy and momentum, the energy that is taken by its atom is very small. Therefore, we will focus on the electron detection.

The energy that is released in this nuclear reaccion is constant, 18.6 keV, but it is divided between the products of this reaccion. Therefore

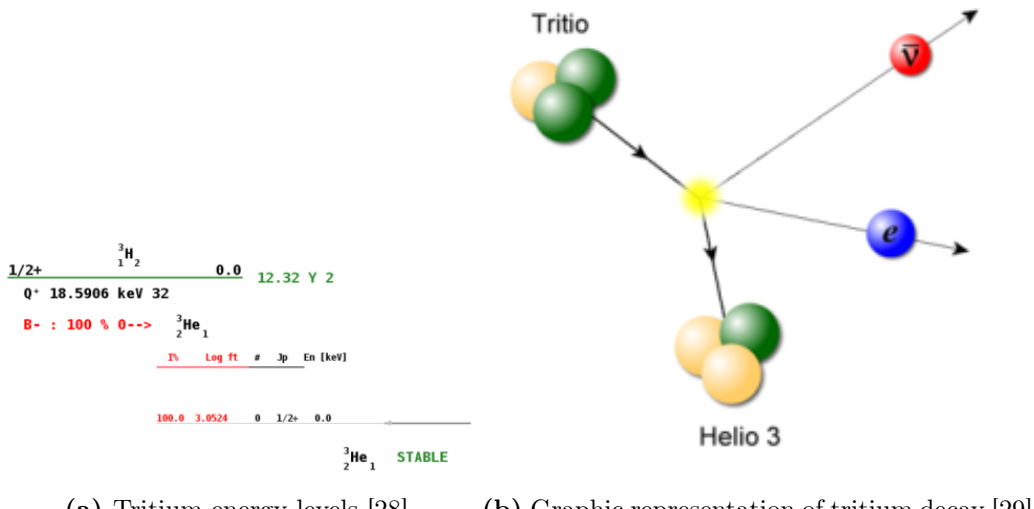


**Figura 1.2 – Tritium decay**

not all beta particle (electrons) will have the maximum energy. This is what we can see in the figure 1.3, which is the energetic spectrum of the electrons which are emitted in the tritium decay. The maximum energy of this electrons is 18.6 keV (when beta particles have all the energy), which is the endpoint energy of this spectrum, the average energy is 5.7 keV and the most likely value is slightly below of the average energy, around 4.5 keV.

Keep in mind that, although the helium isotope is stable, it will be exited immediately after this decay. As a consequence, after the tritium  $\beta^-$  decay, we will have a subsequent deexcitation of the  $^3\text{He}$  which will produce photons,  $\gamma$ , with several well-defined energies that correspond to their energy levels, X-rays. COMPROBAR... It doesn't affect directly to our detector due to the efficiency of our detector at those wavelenghts, as we will see in the section ??, but it could be affect indirectly. BUSCAR ESTAS ENERGÍAS Y VER SI SON TAN DIFERENTES COMO PARA NO AFECTAR DIRECTAMENTE O SE PARENCE A LAS DEL TRITIO Y SI AFECTAN DIRECTAMENTE.

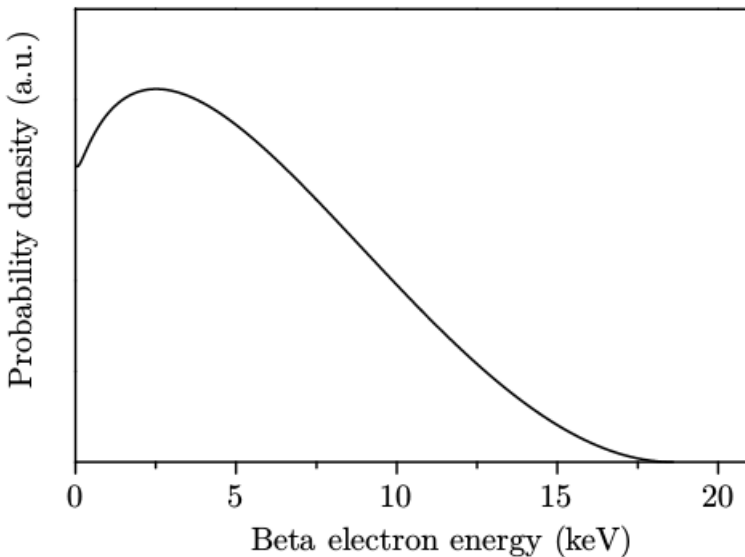


**Figura 1.3** – Energy spectrum of tritium electrons [30]

The releasing energy, which is produced in the tritium decay, is very little. In fact, it is the radioactive isotope with the lowest energy released in its  $\beta$  disintegration [25]. As a consequence the  $\beta$  particles which is emitted in this tritium decay will have a very little mean free path as you can see in the table 1.5.

On the one hand, it means that the tritium electrons is easily stopped even for simply walls like our clothes, the laboratories gloves or even the our skin it-self, that's, the radioactive hazard is low. Nevertheless, the danger of tritium is increased when tritium is ingested or inhaled because if it has enough radiactivity it can affect to our internal organs because it has a high biologic life time, 9.5 days [25], time during which tritium remains in our body and we will be receiving radioactive dose due to tritium radiation. Therefore, their health hazard is high.

On the other hand, this short mean free path will be a problem when we try to detect tritium and due to that, there are some limitations

Material	Energy ( $\beta$ )(keV)	Penetration Depth
${}^3\text{H}_2$ , STP	5.7	0.26 cm
${}^3\text{H}_2$ , STP	18.6	3.2 cm
Air, STP	5.7	0.036 cm
Air, STP	18.6	0.45 cm
Water, soft tissue (solid matter whose density is $1 \text{ g} \cdot \text{cm}^{-3}$ )	5.7	$0.42 \mu\text{m}$
Water, soft tissue (solid matter whose density is $1 \text{ g} \cdot \text{cm}^{-3}$ )	18.6	$5.2 \mu\text{m}$

Table 1.5: Mean Free Path of tritium isotope for several energies and several environments [25]

which we will have to take into account when we design our detector.

Tritium has different physical properties than other natural isotopes of the hydrogen like different boiling points as you can see in the table 1.6 or the property of auto-radiolysis which only happens when radioactive elements are presented. The auto-radiolysis exists because the energy released in tritium decay is larger than the energy bond of oxygen and hydrogen in water molecules (5.2 eV) or the ionization energy of water molecules (12.6 eV) so it can break up these molecules [31]. Due to the auto-radiolysis, some radicals appear in the water whose corrosivity is increased and it is something that we have to take into account when choosing the materials that will make up our detector.

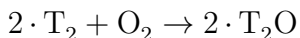
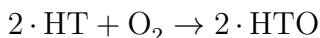
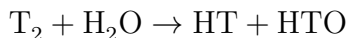
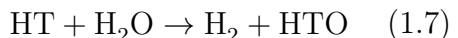
Although tritium has different physical properties it has almost the same chemical behaviour than other hydrogen isotopes. Tritium, like hydrogen, is a gas at STP<sup>1</sup> forming a two-atom molecules which can be HT, DT and T<sub>2</sub>. It can become in tritium water through oxidation and exchange reactions as you can see in the following chemical equations[25]:

---

<sup>1</sup>Standard conditions of temperature (273 K) and pressure (1 atm)

Molecule	Boiling point (for gases) (K)	oxidation form
H <sub>2</sub>	20.39	H <sub>2</sub> O
HD	22.14	HDO
HT	22.92	HTO
D <sub>2</sub>	23.66	D <sub>2</sub> O
DT	24.38	DTO
T <sub>2</sub>	25.04	T <sub>2</sub> O

Table 1.6: Gas molecules of hydrogen isotopes and their boiling points

*Oxidation :**Excahnge*

Due to this chemical similarity tritium water can performe the same chemical process than non-radioactive water, some times with higher rate if the tritium concentration is high enough to catalyze the reaction. Its biological hazard comes from this chemical similarity since tritium water is able to substitute normal water in human body. On top of that, tritium water has a higher absorption in human body, around 99%, than tritium gas, whose absorption in the human body is less than  $5 \cdot 10^{-3}\%$  by inalation or practically negligible by skin absorption [25] so it is more dangerous.

## 1.3 State-of-the-art in tritium detection

Measurement of tritium activity is one of the systematic environmental controls that have been carried out for dozens of years around nuclear power plants during their energy production and around nuclear research facilities.

As a consequence, this measurement has been attempted with many different technologies so far in order to improve the state of the art of each time. The most researched techniques are summarized in the table 1.7.

	LSC	IC	Calorimetry	BIXS
Measured quantity	Scintillation photons	Ionization current	heat	X-rays
LDL	$\sim$ Bq	10 – 100 kBq	$\sim$ GBq	$\sim$ MBq
Sample form	Liquid	Gas, vapor	All	All

Table 1.7: State-of-the-art in the tritium detection for different technics [30]

Nowadays, the most used technic for measuring tritium in water is the LSC. It consists of mixing a liquid sample (some ml for environmental measurements or less for higher activities) with liquid scintillator. In our laboratories, LARAM, at the University of Valencia, this mixture is made in a ratio of 50:50 [32] but it will depend on each system and each sample [33] [34]. In this technic, the  $\beta$  energy that is emitted from the sample excites the molecular energy levels of the liquid scintillator and it is quickly deexcited emitting several photons with a well-known energy (fluorescence), normally in the visible range. Finally these photons are detected with photosensors, processed and analysed.

This technic has a very good detection capability and precision (LDL for tritium better than 1 Bq/L [35]) but it has some problems. On the one hand it needs too much time for taking a measurement (more than 2 days) and,

on the other hand, although this sample could be non-radioactive, it contain toluene which is a toxic chemical waste so we need to follow a special protocol for removing this sample. On top of that all these technics need special staff for sampling, chain-of-custody and lab analysis which consum economical and time resources. In order to avoid the last problem some unsuccessful efforts have been made in order to build a monitor of tritium with LSC [36]. In any case, other problems still remain.

The ionization chamber (IC) is based on a gas chamber (sample) which contains electrodes connected to different voltage. This electrodes recover the ionization current that is produced due to the  $\beta$  radiation. It is a simple and fast system, but the problem is that on the one hand it has too high LDL, more than 10 kBq, and, on the other hand, it needs the state of the sample to be gas or steam [37] [38].

The calorimetry is based on the measurement of the heat generated due to the tritium radiation [39] [40]. The problem with this technic is that it has a too high LDL, of the order of GBq, and it needs too long time, more than 2 days, for taking a measurement.

The Beta Induced X-ray Spectrometry (BIXS) is based on the measurement of the bremsstrahlung with PMTs of NaI [41] [42] or with Silicon Drift Detector (SDD) [43] produced due to the tritium radiation. The problem with this technic is that it has too high LDL, of the order of MBq.

There are many more different methods for tritium detection, although they are less used or less experimentally developed, each one with their own problems for our objective. For example, APD [44], which we cannot use in our case because they cannot function in contact with water, the mass spectrometry [45], which needs to store the sample several months before taking the measurement or Cavity ring spectroscopy [46], which requires a special optical configuration that is not possible outside

the laboratory.

We have to keep in mind that all these techniques are offline methods that take too long to finish the process of taking measurements which include sample taking, sending the sample to the lab, analyzing of the sample so we cannot use them for tritium monitoring. LSC is the only technic which has a LDL enough low to verify the compliance with the established limit, 100 Bq/L. Therefore we will explore this area but, in order to avoid the problems related with this technic (off-line results, no-reusable liquid scintillator and the chemical toxic wastes) we will delve in solid scintillators. There are several studies that have been done so far which intend to do the same as we want with this project, to create a quasi-real time monitor of low tritium activities in water based on solid scintillation:

- First study was done by M. Muramatsu, A. Koyano and N. Tokunaga in 1967 who used a scintillator plate read out by two PMTs in coincidence [47].
- The second study was carried out by the A. A. Moghissi, H. L. Kelley, C. R. Phillips and J. E. Regnier in 1969 that used one hundred plastic fibers coated with anthracene powder and read out by two PMTs in coincidence [48].
- Third study was performed by R. V. Osborne in 1969 who used sixty scintillator plates stacked read out by two PMTs in coincidences [49].
- Fourth study was done by the A. N. Singh, M. Ratnakaran and K. G. Vohra in 1985, who used a scintillator sponge read out by electronic coincidence [50][51].
- Fifth study was carried out by K. J. Hofstetter and H. T. Wilson in 1991, who did different experiments for testing different shapes of scintillator plastic like several sizes of beads, fibers, etc. The better result which Hofstetter got for solid plastic scintillator was a efficiency of the order of  $10^{-3}$  [52][53].

	Efficiency, $\eta_{det}$ (cps/(kBq/L))	Surface $F_{sci}$ (cm <sup>2</sup> )	Specific efficiency $\varepsilon_{det} =$ $\eta_{det}/F_{sci}$	LDL (kBq/L)
Muramatsu	$3.85 \cdot 10^{-4}$	123	$3.13 \cdot 10^{-6}$	370
Moghissi	$4.5 \cdot 10^{-3}$	> 424.1	$< 1.06 \cdot 10^{-5}$	37
Osborne	0.012	3000	$4 \cdot 10^{-6}$	37
Singh	0.041	3000	$1.37 \cdot 10^{-5}$	< 37
Hofstetter	$2.22 \cdot 10^{-3}$	~ 100	$< 2.22 \cdot 10^{-5}$	25

Table 1.8: Results of different scintillator detector for tritium detection [30]

The results of these experiments are summarized in the table 1.8. We can see in the first column that the intrinsic detector efficiency,  $\eta_{det}$ , is very different in these experiences. As we know that, in this type of detectors, one of the most important factor, which affect to the efficiency, is the active surface of the plastic scintillator,  $F_{sci}$ , and we can see in the second column that it is very different in each detector, we use the specific detector efficiency (third column), in order to compare these experiments, that's, the intrinsic detector efficiency normalized to this active surface. Now we can check that, effectively, these specific efficiencies are quite similar. On top of that we can check that the better specific efficiency was obtained for Moghissi who used scintillating fibers. This is a good point which justify our choice about using of fibers like a scintillator. Finally we can see in the last column that the LDL in all these experience are more or less similar and, they are too high for our aim so developing a detector which overcome these LDL is an essential study right now in order to monitoring the tritium levels.

## 1.4 Tritium project and Tritium monitor

As we have seen in the section 1.3, the current technics which exist nowadays have either higher LDL than the limit established by Council Directive, 100 Bq/L, or they are a off-line method (too slow) so those methods cannot be used for tritium monitoring in quasi-real time.

As a result of these limitations appear the *Tritium* project [54], whose title is "Design, construction and commissioning of automatic stations for quasi-real time monitoring of low radioactive levels of tritium in water".

This project has been funded by Interreg Sudoe program of the EEC in the 2016 call with the reference number SOE1/P4/EO214. The purpose of this project is the development of a tritium monitor in quasi-real time. This monitor consists of a ultrapure water system, which prepare the sample before we introduce it in our detector, the tritium detector where the tritium measure will be done, the active veto and the pasive shielding which reduce the natural background of our tritium detector and several types of electronic which control all these parts of the monitor, analyze the tritium measurement and will send an alarm if the limit of 100 Bq/L is overcome.

The tritium detector is based on measurements of low energy beta radiation from the radioactive decay of tritium. For doing this task this detector consists of scintillator fibers, that we put directly in contact with water which can contain tritium. We need to put both, scintillator fibers and tritium water, in contact due to such a low mean free path of tritium electrons (table 1.5 of the section 1.2). Then, the photons produced on this fibers will be read out by several photosensors. The photosensors which we have tested in this experiment are photoelectron multiplier tubes (PMT) and silicon photoelectron multiplier (SiPM) arrays.

The difficulty when we try to measure tritium is to distinguish these signals from the background. This is because tritium signals are small since tritium events has low energy ( $\sim$  keV) and this is the energy range in the spectrum where there are more background counts (the lower energy in the spectrum, the more electronic noise). We will use coincidence techniques in order to reduce the counts from the background.

It is important to check the water tightness of each prototype because if the water reaches the photosensor it will be irreparably damaged. On top of that if we use high concentrations of tritium in water for laboratory tests we can contaminate this laboratory, which could be dangerous for the healthy of the workers and it could spoil measurements of future experiments.

Finally this monitor will be installed in the Arrocampo dam, Almaraz, Spain, where the Almaraz nuclear power plant release the water which is used in their cooling system, Figure 1.4. This NPP has two nuclear reactors whose type is PWR. This dam is located near the Tajus river, which is the largest river in Spain, 1007 km. This river cross from Aragon (Spain) to Lisbon (Portugal) and flows into the atlantic ocean. This river is used for an important quantity of animals, plants and even humans because the water of this river is used as drinking water by the spanish and portuguese people. Therefore the international cooperation in order to maintain the quality of this water is very important.

The *Tritium* collaboration is a international group consisting of a consortium of 6 different southwestern european institution of 3 different countries: The University of Aveiro, in Portugal, The University of Bordeaux and the CNRS (Section Aquitaine-Limousin), in France and the University of Extremadura, *Junta de Extremadura* and University of Valencia, in Spain.

## FOTOOS PERSONAS TRITIUM



(a) Arrocampo dam and Almaraz Nuclear Power Plant      (b) Tajus river along Spain and Portugal

**Figura 1.4 – Arrocampo dam, Almaraz NPP and Tajus river**

Each institution has focused in the development of a different part of all this project:

- First, the Extremadura group has developed and installed the ultra-pure water system with which we get water with very low conductivity,  $\sigma \approx 10 \mu\text{S}/\text{cm}$ . The conductivity of the water before the cleaning process is around  $1000 \mu\text{S}/\text{cm}$ . This clean process is very important for two reasons. On the one hand, it is important for maintaining our detector very clean, which is a critical point. On the other hand, it's important because with this process we reduce the natural background since we remove several natural radioactive isotopes that there are in this water (except tritium) such as  $^{222}\text{Rn}$ ,  $^{40}\text{K}$  or  $^{137}\text{Cs}$ . This system will be explained in the section 2.3.
- Second, french group has developed the passive shielding where our detector will work inside. It is based in ultra radiopure lead with very low intrinsic activity. The objective of this passive shielding is to reduce the external natural background that affects to our system, for this reason we use lead. Obviously, this shielding doesn't have to affect to the measurement of our system, for this reason we use radiopure elements with very low intrinsic activity. This shielding will be explained

in the section 2.4.1.

- Third, The Portugal and Spain people has collaborated for designing, developing and building four different prototypes of tritium detector and active vetos for removing cosmic events. These prototypes and vetos will be explained in the chapter 4 and section 2.4 respectively.
- Lastly, The Portugal and Spanish people has also developed the simulations about this system. The program which we have used in this project is GEANT 4, which is a simulation package. It consists in a extensive C++ library with which we can design the geometry of our detector, the physical processes which happen there, etc. This simulation will be explained in the chapter 5.

The tritium level which we want to measure follow the ALARA principle (As Low As Possible Achievable) and to get it there are important characteristics which our tritium detector must have:

- *Compact.* This is important because in the place where this detector will be installed the useful space that we can use is finite.
- *Thin active volume and large active area.* On the one hand, we have to take into account that, as we have seen in the table 1.5 of the section 1.2, the mean free path of the  $\beta$  particle of tritium decay is very low so we need to work with thin active volumes. In the practice, Active thickness beyond the mean free path of the tritium will only contribute to the background. On the other hand, as we have checked in the section 1.3 the efficiency of this type of detector scales with the active area so we need to design our detector with the largest possible active area.
- *High sensitivity to tritium.* We are going to work with low tritium activities so we need to reduce as much as possible the non-detected tritium events.

- *High specificity to tritium.* We need that our detector is able to distinguish the tritium signal of the signal of other radioactive elements which can be present in the initial sample.
- *Quasi-real time response.* As we have seen it is important that our system can work in quasi-real time in order to detect any problem as fast as possible.
- *Rugged system.* Finally, we have to take into account that our objective will be installing an automatical system which will work during a lot of years without specialized people so we need that our monitor are rugged.

In order to get the measurement in quasi-real time we need to work *in situ*, that's, we need that our detector is able to work in the same place that we take the sample. Whit the work *in site* we achieve:

- a faster monitor because we eliminates the process of taking the sample, the chain-of-custody until this sample arrive to this laboratory and the complexity which involve these tasks.
- a better monitor since if we can work *in site*, our measurements can be more frequent hence we will can identify cahnges in the activity earlier.
- a cheaper monitor because we have not only the material costs attached to the sample collection, chain-of-custody of this sample, shipping of this sample to the laboratory, etc. but we have also eliminated the costs attached to the specialized staff who are involving in these tasks. Our detector will only need frequent calibrations each time in order to ensure its correct operation.
- a safer monitor since the personal exposure dose is reduced and the changes in activity are detected fastly. On top of that we remove the possibles mistakes which can be done by specialized staff.

## **1.5 Work scheme**

# Chapter 2

## Design principles of the Tritium monitor

### 2.1 Detector system overview

The objective of the TRITIUM project is the design, development, construction and commissioning of an automatic station for real-time monitoring of low levels of tritium in water. To achieve this objective, the TRITIUM experimental group has developed a monitor that is based on several parts that will be explained in the sections contained in this chapter. The different parts which is contained in our monitor are:

- The tritium detector, chapter 4, that is based on several modules that are read in parallel. Each module consists of hundreds of scintillating fibers, section 2.2.2, read by two coincident photosensors, section 2.2.3. These scintillation fibers are directly in contact with the water sample whose tritium level we intend to measure and the photosensors included in this study are photomultiplier tubes (PMT), section 2.2.3,

or silicon photomultipliers (SiPM), section 3.2.

- The ultrapure water system, section 2.3, that is used to condition the water sample before the measurement. This system removes all the organic particles that are dissolved in this water and all the particles whose diameter is greater than  $1 \mu\text{m}$  without affecting the level of tritium in the sample. It is important for two reasons, on the one hand because, as we have seen in the section 1.2, the mean free path of tritium in water is very short, 5 or  $6 \mu\text{m}$  so it is important to avoid the deposition of this particles in fibers because this would prevent us from tritium detecting. On the other hand some of this particles dissolved in the water sample are natural radioactive particles that would increase the background of our detector if we didn't remove it and, due to the fact that we have few tritium events in our samples, it is very important to reduce the background of our detector as much as possible.
- The background rejection system, chapter 2 that is based on two different parts. On the one hand we use a passive shield, section 2.4.1, that consists of a lead castle inside which we use our detector. It is used to eliminate the natural radioactive background that is found in the place where we use the Tritium detector, generally the events with relatively low energy ( $< 200 \text{ MeV/nucleon}$ ). On the other hand, we use an active veto, section 2.4.2, consisting of two (or more) plastic scintillation blocks, each read by two of the chosen photosensors. This active veto is inside the passive shield and the tritium detector is placed between both plastic scintillation blocks. This active veto is important because there are high energy events ( $> 200 \text{ MeV}$ ), such as cosmic events, that can travel through the passive shield and affect to the measurement of our detector. Contrary to what happens with low energy events, it is difficult to avoid that these high energy events arrive to our detector. What we will do with this active veto is to detect these high energy events and, for each of them, open narrow time

windows in which we will not read the Tritium detector to prevent these events from affecting the tritium measurement.

- A general electronic system, section ??, that will be used to monitor all the different parts of this monitor and send an alarm if the tritium level limit, which has been set for us (100 Bq/s), is exceeded.

When this monitor is working and several tests have been passed with which we can verify that it works correctly, it will be included in the existing early warning system in Extremadura, which consists of various types of radioactive detectors whose objective is to monitor the status of the environment around various locations including the Arrocampo nuclear power plant.

## 2.2 Tritium detector

Due to the reasons which we have discussed in the section 1.3, the type of the detector which we have developed in order to measure the tritium that there is in water samples is a scintillator detector. It consists in a chain of three main elements:

- The scintillator, that is the material in charge of detecting the tritium event. The tritium particle or a general particle (ionizing radiation) hit this material and deposits part of their kinetic energy (or all, as in the case of the tritium event) in it through ionization and excitation. Part of this energy deposited is converted in photons, generally in the visible range.

The number of photons produced carry information about the particle detected, such as its energy, type, etc.

- The photosensor, which is the part of the detector in charge of detecting the photons produced by the scintillator that reach its sensitive element (the more scintillated photons arrive to your photosensor, the better signal you have in your detector).

The most used photosensor in nuclear physics are SiPMs and PMTs which detects some of the photons produced in the scintillator and transforms it in electrons which are multiplied with a factor of around  $10^6$ . This millions of electrons form a electronic pulse whose properties has information of the photons that has been detected.

- The electronic system, which is the part of the scintillator detector in charge of processesing and analyzing (first analogically and then digitally) this electrical pulse of the photosensor to give us useful information about the event detected that we can understand and interpret such as a number, for instance the activity, or some kind of spectrum like energy spectrum.

In figure 2.1 we can see the scheme of a scintillation detector where the scintillator material detects ionizing radiation and produces photons that will be guided by the reflector and the light guide to the photosensor. There, some of the photons that reach the sensible part of the photosensors will be converted and multiplied into millions of electrons that will form a electronic pulse. The output signal of the photosensor (electronic pulse) will be processed and analyzed by the corresponding electronics:

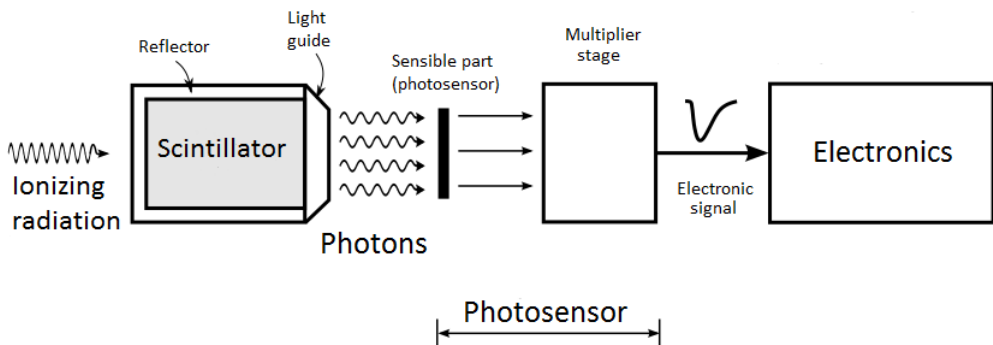


**Figura 2.1** – Scheme of the scintillator detector [?]

### 2.2.1 Interaction of fast electrons and photons with matter

In this section, the explanation will only focus on the particles and energy range that are interesting for this thesis, which are electrons ( $0 - 18$  keV) and photons in the visible range (approx.  $380 - 750$  nm).

On the one hand, electrons have charge so their interaction with matter are mainly produced with the orbital electrons that there are in that matter due to the Coulomb force. The trajectory which electrons follow is much more tortuous than other heavier particles because the mass of both interacting particles is equal, electrons. Furthermore, for the same reason, these electrons lost a significant amount of energy in each collision.

In order to speak about the total energy lost of particles in matter the specific energy loss is defined as  $S = -\frac{dE}{dx}$  which expresses the energy loss suffered by the particle per unit of trajectory. In the case of electrons, this total energy loss has two main contributions, the collisions (elastic and inelastic) and radiative processes (bremsstrahlung):

$$\frac{dE}{dx} \approx \left( \frac{dE}{dx} \right)_c + \left( \frac{dE}{dx} \right)_{br} \quad [55][56] \quad \frac{\left( \frac{dE}{dx} \right)_{br}}{\left( \frac{dE}{dx} \right)_c} \approx \frac{EZ}{700} \quad [55] \quad (2.1)$$

Where  $E$  is the energy of the electron in MeV and  $Z$  is the atomic number of the absorbing material. Due to this energy loss, the electrons can only penetrate a material as far as they go before losing their total kinetic energy. This distance is known as range and, in the case of tritium electrons, its value is seen in the table 1.5.

On the other hand, photons don't have charge. Its possible interactions with the matter are photoelectric effect, Compton effect, coherent

scattering and pair production and the probability of each process depends on the energy of the photon,  $E_\gamma = h\nu$ , and the atomic number of the material, Z, as you can see in the figure 2.2.

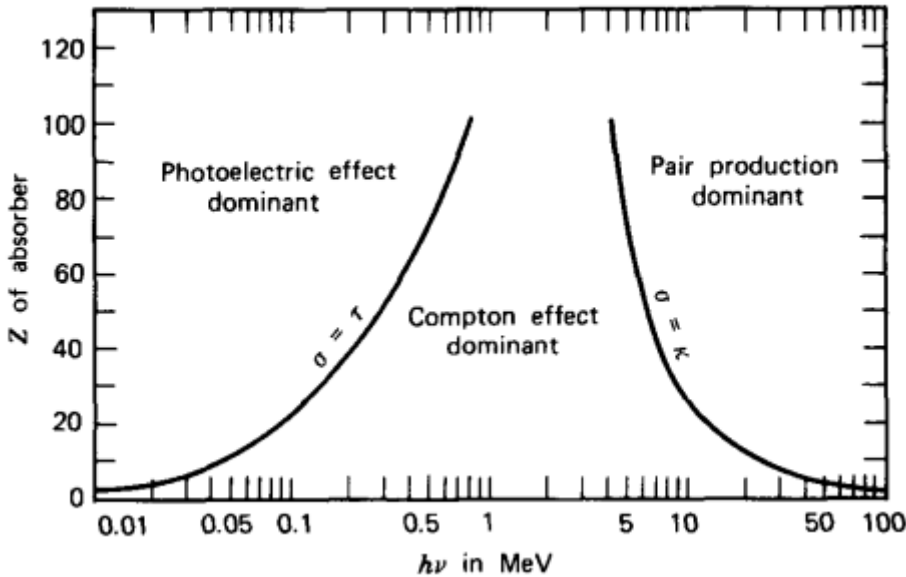


**Figura 2.2** – Domain regions of the three most probable types of interactions of gamma rays with matter. The lines show the values of Z and  $h\nu$  where the two neighboring effects are equally likely. [55] [56]

We have to take into account that the only relevant photons for this thesis are in the visible range, between 400 and 700 nm, that corresponds with energies of the order of the eV. Therefore the last effect, pair productions, will be not explained here because it needs a photon energy equal or more than 1.022 MeV for happening and it is not our case.

The photoelectric effect occurs when a photon interacts with an orbital electron in the material, losing all its energy. This energy is absorbed by the electron that is released from the atom (ionization). The energy of the resulting electron,  $E_e$ , is:

$$E_e = E_\gamma - E_b \quad [55][56] \quad (2.2)$$

Where  $E_b$  is the binding energy of the electron in this material. The probability of this effect depends on the number of available electrons through the variable  $Z$ , and the energy of the electron according to the following expression:

$$(Pr)_{Ph-eff} \approx \frac{Z^n}{E_\gamma^{3.5}} \quad [55] \quad (2.3)$$

As we can see in this expression and in the figure 2.2, the photoelectric effect is most probably if we use elements with high atomic number. This is the reason why elements with high atomic number are the best insulators against gamma radiation and this is one of the reasons why we use lead ( $Z = 82$ ) for building our passive shielding as we will see in the section 2.4.1. This is also the reason why elements with high atomic number are used in the cathode of PMTs.

The Compton effect occurs when the photon interacts with an orbital electron of the material, transferring part of this energy to the electron, which is released, and this photon is scattered at an angle  $\theta$  with respect to the original direction. If we neglect the binding energy, the energy transferred to this electron,  $E_e$ , is shown in the following equation:

$$E_e = \frac{\frac{E_\gamma^2}{m_0 c^2} (1 - \cos\theta)}{1 + \frac{E_\gamma^2}{m_0 c^2} (1 - \cos\theta)} \quad [55][56] \quad (2.4)$$

Where  $m_0$  is the rest mass of the electron and  $c$  is the speed of the light in the vacuum. The probability of the Compton effect is proportional to the atomic number (more available electrons),  $Z$ , and decreases with the

energy of the photon.

As we can see in the figure 2.2, in the energies of the photons belonging to the visible range of the electromagnetic spectrum (of the order of eV), the Compton effect is only more likely in very light materials, ( $Z < 4$ ). For heavier materials the photoelectric effect is the dominant effect.

Finally, in the coherent scattering, the atom is neither excitation nor ionization and the photon conserve all their energy in this collision. This effect is more probable for photons with low energies and materials with high atomic numbers. Because of the fact that the energy of the photon doesn't change we will not speak more about this effect but it is important since this effect changes the direction of photons and it will affect to their mean free path.

### 2.2.2 Scintillators plastic

The use of scintillators in radiation detection is one of the most used techniques in nuclear physics. The scintillator is a material that is able to convert the kinetic energy of the incoming particles in light <sup>1</sup> which we can detect and quantify. It happens because the radiation excites and ionizes the scintillating atoms which, after that, are immediately de-exciting (with times of the order of picoseconds), emitting photons.

This conversion should be linear in a wide energy range of incoming particles and it is necessary that this material has good optical properties, such as being transparent to the wavelength of their own emission and having a refractive index as close as possible to the glass for optimizing optical coupling with photosensors.

The photon emission in the scintillator is a statistical process,

---

<sup>1</sup>Photons in the visible energy range

which means that two exactly the same events will emmit different number of photons. It follow a poisson statistics so when we speak about the number of emmited photons we speak about the mean number of photons.

There are two types of scintillators, organics and inorganics. Inorganic scintillators normally have a higher atomic number and density so their light output are higher. Due to these reasons they are better for gamma-ray spectroscopy (take into account figure 2.2). Organic scintillators are generally faster and they are commonly used for beta spectroscopy and neutron detection. In this section I focus my explanation mainly on organic scintillators since they are the ones we have used in our research.

Organic scintillators are based on a scintillator material, which produces light, dissolved in a base solvent. This solvent is normally based on aromatic hydrocarbons (carbon atoms linked together), that is, they are mainly composed of carbon and hydrogen atoms as we can see in the molecules of some of the most widely used scintillators,  $C_{18}H_{14}$ ,  $C_{24}H_{22}N_2O$  or  $C_{15}H_{11}NO$  whose average atomic numbers are between 3,5 and 5.

The scintillator molecules, in which the organic scintillators are based, have the so called  $\pi$ -electron structure. The energy levels of their electrons are commonly illustrated with a Jablonsky diagram, figure 2.3, where we can see the fundamental single state,  $S_{0i}$ , where the valence electrons are, the excited single states,  $S_{jk}$ , and the excited triple states,  $T_{lm}$ . De energy difference between  $S_1$  and  $S_0$  states is around 3 or 4 eV, energy range of the visible photons. We can see in this diagram that each of this energy states are subdivided in smaller energetic sublevels whose distance between them are around 0.15 eV. This finer energy structure is due to the excitations of molecular vibrational modes and they are expresed with the second index of the energy states.

Because of the reason that the distance between all energy levels and sublevels are larger than the termal energy, 0.025 eV, non-exciting

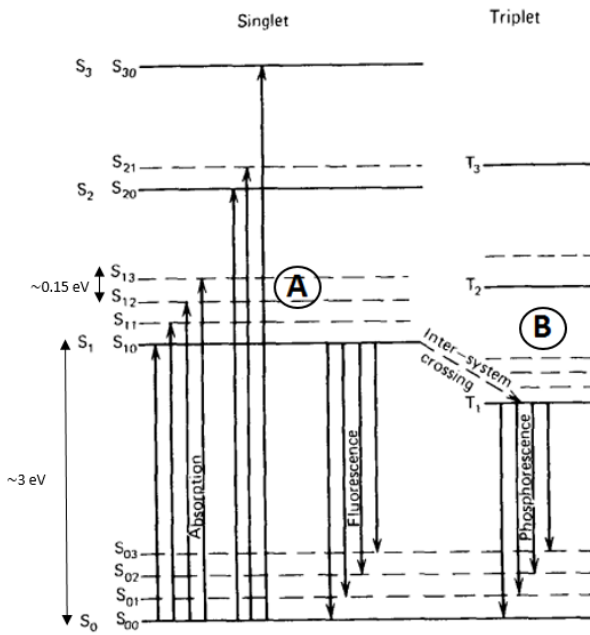


**Figura 2.3 – Jablonsky diagram.** [55]

electrons are in the lowest state  $S_{00}$  at STP <sup>2</sup>.

When a particle deposits their kinetic energy on a scintillator, their valence electrons are exited to higher single energetic states very fast (times of the order of picoseconds) which is expressed with upwards direction arrows in the figure 2.3 and they are quickly de-excited to the first single excited state,  $S_{10}$ , through non-radiative processes known as internal conversion.

Now, this electrons can de-excited to the fundamental single state,  $S_{00}$ , through three different physical mechanisms:

- The prompt fluorescence(process A in figure 2.3), where the electron in the  $S_{10}$  energy level is de-excited to some sublevel of the fundamental state ( $S_{01}, S_{02}, S_{03}$ ).

<sup>2</sup>Standar temperature conditions

tal state  $S_{0i}$ , emitting a photon with an energy equal to the energy difference of these levels (around 3 or 4 eV, visible light). This process happens immediately after the excitation of the scintillator molecules (around tens of nanoseconds after excitation). Each scintillator has a characteristic emission spectrum that defines its response due to the fluorescence mechanism.

Now we can understand why organic scintillators are practically transparent to their own fluorescence emission. This is because of the reason that there exist a quenching effect in each de-excitation process whereby there is a loss of radiated energy. Due to that, all emitted photons by the scintillator have less energy than the required energy for excitation. This effect is called Stokes shift and it's represented with a general wavelength spectrum in the figure 2.4.

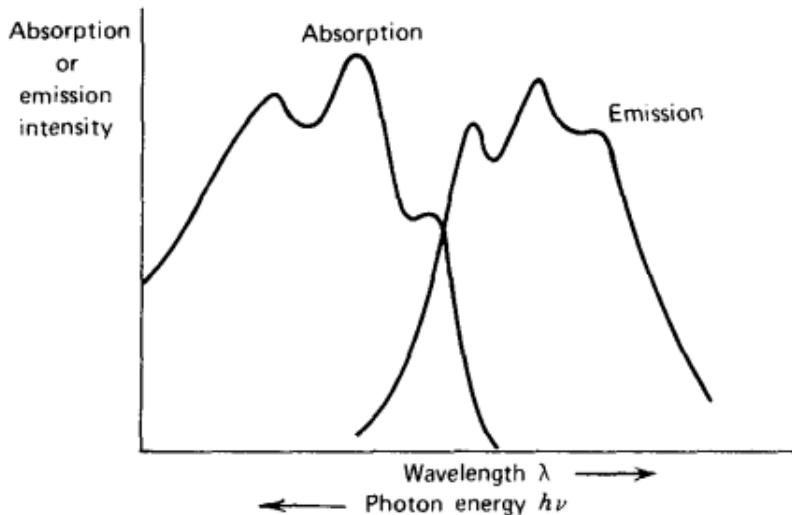


**Figura 2.4 – Stokes shift. [55]**

One of the most important parameters in nuclear physics is the scintillation yield, which is the fraction of particle energy that is converted in light. All mechanisms which don't produce prompt fluorescence, like phosphorescence or delay fluorescence, which we will see later, or

even internal conversion, contribute to reduce this parameter. The signal of the scintillator depends on the type of particle so, the scintillation yield will be different. This factor is normally given by the manufacturer for mips<sup>3</sup> in number of photons per MeV.

The intensity of the fluorescence emission in an organic scintillator during time is a combination of two exponential functions, one associated with the lifetime of the level,  $\tau$  (on the order of nanoseconds), and the other associated with the energetic level population,  $\tau_1$  (on the order of picoseconds).

$$I = I_0 (e^{t/\tau} - e^{t/\tau_1}) \quad [55] \quad (2.5)$$

- The phosphorescence, where the electron that is in the first single excited state cross to a triple excited state (process B in figure 2.3) with a process called "intersystem crossing". This is a metastable state with a much longer lifetime so electrons in this state are de-excited to the  $S_{0i}$  state, emitting a photon much later than phosphorescence. This process can happen up to  $10^{-3}$  seconds after scintillator excitation.
- Delayed fluorescence, which occurs when an electron is in a triple excited state but whose transition to the ground state is forbidden. In this case, this electron can interact with another that is in a similar state and return to the first single state ( $S_1$  is a more energetic level than  $T_1$ ) and quickly de-excited to the ground state.



This emission has the same emission spectrum as immediate fluorescence, but occurs later.

The scintillating detectors generally use the prompt fluorescence

---

<sup>3</sup>Minimum ionized particles, that's, for example, electrons with 500 keV or more

light as output signal so a good scintillator should increase it and reduce other possible physical mechanisms.

Plastic scintillators are organic scintillators that has been dissolved in a solvent and polymerized. They are easy to machine and can take any desired shape during construction. Among the forms most used today we can find blocks, thin sheets, cylinders, etc.

In our experiment we have been working with an plastic scintillator in the form of fiber, specifically, commercial fibers BCF-12 from Saint-Gobain Crystals Inc [57]. This type of fiber was chosen as the result of a comparative study among some of the best-known commercial manufacturers [58], such as Kuraray [59].

The BCF-12 fibers consist of a scintillated core, whose material is polystyrene, one of the most used solvents for plastic scintillators [55], with the possibility of surrounding it of a cladding of polymethylmethacrylate (PMMA) (smaller refractive index than core in order to achieve a critical angle) or a multicladding (second cladding) with even smaller refractive index.

When a particle deposits all or part of its kinetic energy, some photons are produced in the fiber core as a result of the scintillating process. The quantity of photons which are produced depend on the scintillation yield, whose value is around 8000 photons per MeV for a mip in our case (BCF-12 fibers). It means that, for instance, for tritium electron, this fibers will release a maximum of around 148 photons (when tritium electron has the maximum energy, 18.6 keV), probably less because electrons with these energies are not mips.

These photons will shape the useful part of the response of the scintillator (fluorescence) for us. The energy (or wavelength) of these scintillated photons follows the distribution of their emission spectrum which, for the used fibers, is shown in the figure 2.5.

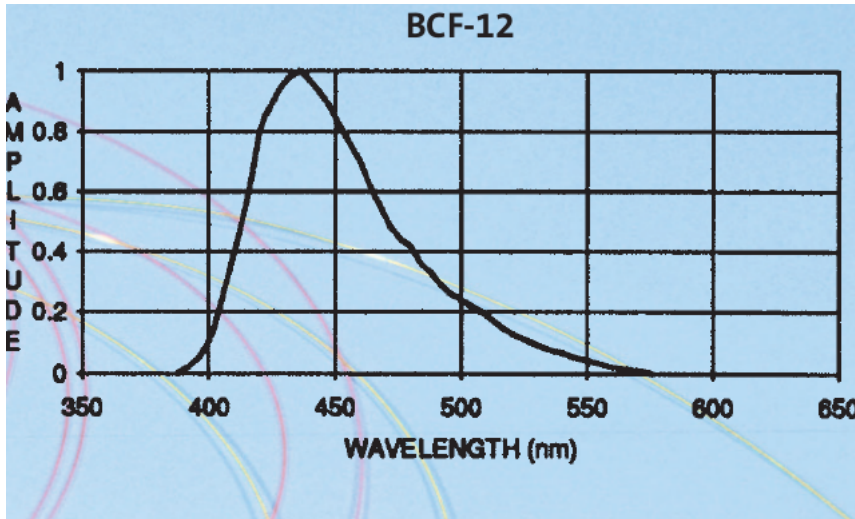


**Figura 2.5** – Emission spectrum of BCF-12 fibers of Saint-Gobain. [57]

After the production of scintillated photons, we need to guide these photons to the sensitive part of the photosensor where we will detect them with some probability. Fibers (and scintillators in general) use the optical property of Snell's law [60] to guide their photons to the desired part (the ends of the fibers). It is based on the interface created between the core and the surrounding material. When a photon hits this interface, it is refracted (and therefore lost) following the Snell equation, 2.7. If the surrounding material has a lower index of refraction than the core of the fiber, there exist a critical angle,  $\theta_c$ , at which, for angles equal or larger than this one, the photons will be totally refracted (and therefore conserved in the fiber for being guided). This effect is showed in the figure 2.6.

$$n_0 \operatorname{sen}(\theta_0) = n_1 \operatorname{sen}(\theta_1) \longrightarrow \theta_c = \operatorname{asen} \left( \frac{n_1}{n_0} \right) \quad (2.7)$$

There exist a parameter which define the efficiency of the scintillator in order to guide photons, the trapping efficiency. For BCF-12 fibers is between 3.44% and 7% (depending if the event was detected near the fiber

axis (minimum) or near the core-clad interface(maximum)).

Therefore, from these 148 photons initially created with the tritium electron with the maximum energy, only a maximum of around 10 photons (for maximum trapping efficiency) will arrive to our photosensor. As you can see, we work with very weak detector signals, where there is more electronic noise and, as you will see in future chapters, we have made a big effort to reduce this electronic noise as much as possible with several technics.

In the figure 2.6 we can see how a scintilalting fiber works.

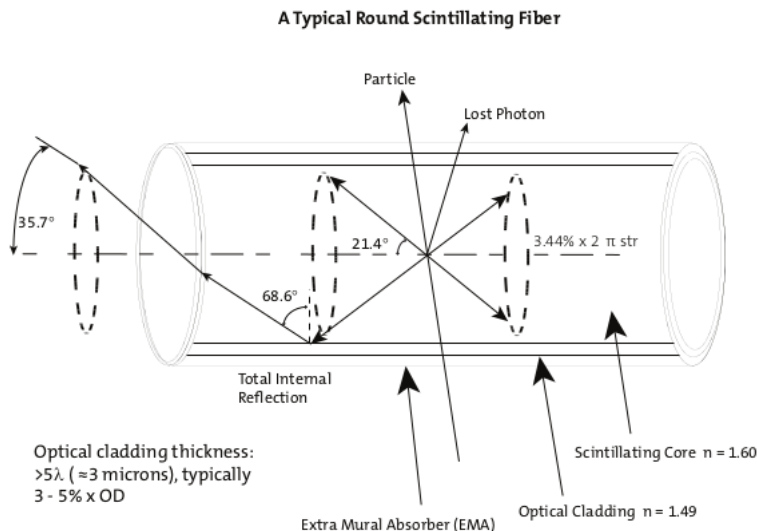


**Figura 2.6** – How photons are collected in a fiber with single clad. [57]

The cladding material is useful for protecting the core surface from dirt or aggressive external agents that can reduce the light collection but at the cost of losing some light because it increase the critical angle. In the table 2.1 we have three different examples where this effect is illustrated.

This is what theoretically happens but, in the practice, it's difficult to achieve a perfect air-core or water-core interface and it will affect to the light collection. Due to the reason that the commercial claddings are thicker

Material	Refractive index	critical angle ( $^{\circ}$ )
Air	1	42.98
Water	1.33	62.47
Cladding of PMMA	1.49	76.26

Table 2.1: Critical angles associated to different interfaces created with polystyrene,  $n_0 = 1.6$ , and other materials

(30  $\mu\text{m}$ ) than the mean free path of tritium in water ( around 5  $\mu\text{m}$ ) we cannot use commercial cladding in our detector hence we will need to take special attention for achieving a water-core interface enough good. As we will see in the section ??, we have used a special protocol developed in the ICMOL (pie de pagina explicando que es el ICMOL) for preparing fibers before we use them for tritium detection.

Some of the most important properties of the used fibers are summarized in the table 2.2.

Core material	Polystyrene
Core refractive index	1.60
Density ( $\text{g}/\text{cm}^3$ )	1.05
Cladding material	Acrylic (PMMA)
Cladding refractive index	1.49
Cladding thickness ( $\mu\text{m}$ )	30
Numerical aperture	0.58
Trapping efficiency	3.44% minimum
Radiation length (cm)	42
Emission peak (nm)	435 (Blue)
Decay Time, (ns)	3.2
$1/e$ Length (m)	2.7
Scintillator yield ( $\#\gamma/\text{MeV}$ )	$\sim 8000$
Operating Temperature	$-20^{\circ}\text{C}$ to $50^{\circ}\text{C}$

Table 2.2: Properties of BCF-12 fibers from Saint-Gobain Inc. [57]

### 2.2.3 The light detection in photosensors

So far we have created the scintillating photons in the core of the fiber, which have been guided to its ends. Now, what we need is the so-called photosensor, which is an element that is able to detect these scintillating photons. Photosensors have a sensitive part that is optimized to detect photons in a range of energy (normally inside of a visible range<sup>4</sup>) with enough efficiency. After that, the photosensors create an electronic signal that carries information about these photons detected, such as their number or their detection time.

One of the most important things in the scintillation detector is that the emission spectrum of the scintillation (figure 2.5 in our case) overlaps as much as possible with the detection efficiency spectrum of the photosensor used, specifically their higher peaks. In this case, the efficiency of this detector, which is proportional to the multiplication of both factors at the same photon energy, will be optimized (the largest).

There are a lot of different photosensors that can be used for this purpose, whose photon detection relies on totally different physical processes, such as photoelectron multiplier tubes (PMTs), silicon photoelectron multiplier (SiPM) or charge-coupled device (CCD). Each one of these will have different properties and we have to choose the one which fit better for our objective.

Our main proposal for our scintillation detector will be to use SiPM arrays because they are very fast (of the order of nm) and have high photodetection efficiency (a maximum of around 50%) and high gains (multiplication factor of  $10^6$ ) with a low voltage supply. On top of that, one of the most important reason of this choice is that SiPM arrays are able to detect a single photon with high efficiency, which is very important since, as we have seen in the section 2.2.2, just a few photons will arrive to the

---

<sup>4</sup>Photons whose wavelength is between 380 nm and 750 nm

sensible part of the photosensor. We will test also the PMTs, which are the conventional choice, because they are still interesting since they have lower dark count rate than an equivalent SiPM and some similar properties like its gain.

### Photoelectron multiplier Tubes (PMTs)

Photoelectron multiplier tube is one of the most used photosensors in nuclear physics during last decades. Its main objective, like all photosensors, is to detect the scintillating photons that reach its sensible part and convert it in an electronic signal large enough to be measured.

In the figure 2.7 we have a schematic drawing where we can see the PMT components and how it works. First of all, as we can see in the figure 2.7, we need to create electrons that will travel in the medium (electronic signal). To increase the amount of conserved electrons, we need to work inside a vacuum tube. Therefore, the PMT consists of a vacuum tube that has a glass window through which photons will penetrate inside.

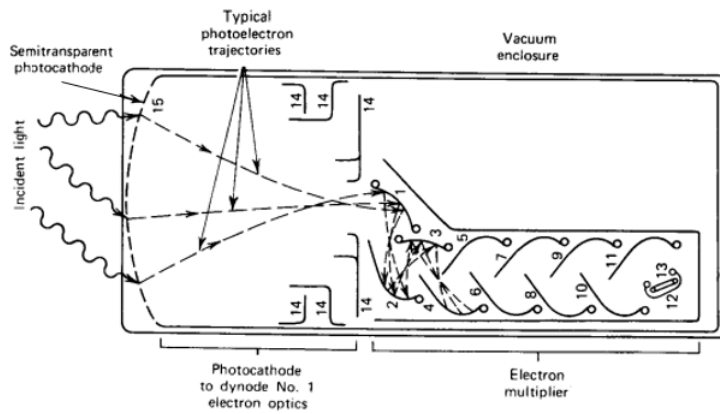


**Figura 2.7** – Scheme of a PMT. [55]

The way in which PMT achieves their aim of detecting scintillating photons happen inside this vacuum tube and it is based in two different

phases:

- First, the PMT convert photons that reach its sensible part in electrons, called photoelectrons, with some probability through photoelectric effect. This sensitive part is the photocathode, which consists of a thin layer (thickness of the order of nanometers) deposited on the inner surface of the PMT windows. The material of the photocathode is chosen to increase the probability of producing photoelectric effect with the scintillating photons. The PMTs which we have used in this experiment are the model R8520-406 from Hammatsu [62]. The material of the photocathode in our case is Bialkali.

The response of the PMT at long wavelengths is limited mainly because the photon does not have enough energy to produce a photoelectric effect or the emitted photoelectron does not have enough energy to overcome the material-vacuum interface. The response of the PMT at short wavelengths is limited mainly due to absorption in the window material, quartz in our case. Due to both reasons, the response of the PMT will have a strong dependence with the energy of the photon and it's commonly expressed in the quantum efficiency (QE) spectrum which is the quotient between the number of photoelectrons produced at the cathode of the PMT and the number of photons reaching it. For our PMTs, is showed in the figure 2.8.

The maximum values of the PMT quantum efficiency is commonly between 20% and 30% [55] (a little bit less than 30% in our case [62]). If we compare the emission spectrum of our scintillating fibers, figure 2.5, with the quantum efficiency spectrum of the PMTs that we have uses, figure 2.8, we can see that the peaks of the spectrum are more or less in the same position (435 nm for the fibers and 420 nm for the PMT and approximately the same value for 435 nm). As I said in the subsection 2.2.3, it is very important for increasing the overall efficiency of our scintillation detector.

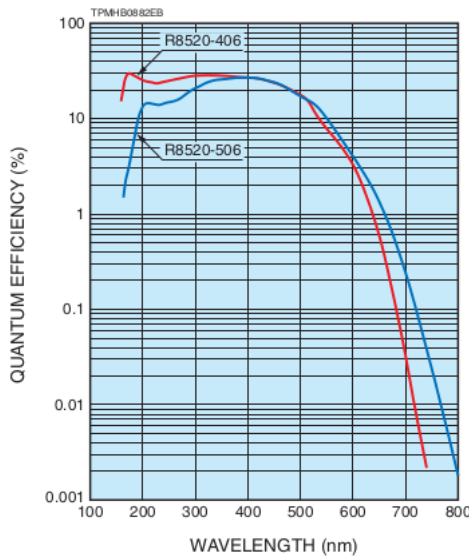


**Figura 2.8** – Quantum efficiency spectrum for the PMT used (R8520-ZB277). [62]

- Next, Due to the reason that the number of photoelectrons in the photocathode is very small, we need a electron multiplication stage to achieve a large enough electronic signal to be processed by the electronic system.

This stage is based on three elements, focusing electrodes, dynodes and anode: They are metallic sheet whose shape and position are designed to optimize the collection of the electrons. The PMT needs a high voltage (HV) which are distributed between all this elements, including the photocathode, in a increasing voltage way in order to attract and accelerate the electrons. This voltage division is achieved with an electronic circuit than can be fed with positive voltage (ground in the photocathode) or negative voltage (ground in the anode). The comercial electronic circuits of Hammatsu are showed in the figure 2.9.

The electronic circuit that can be supplied with negative voltage is faster due to the ausence of the capacitances C4 and C5, but the

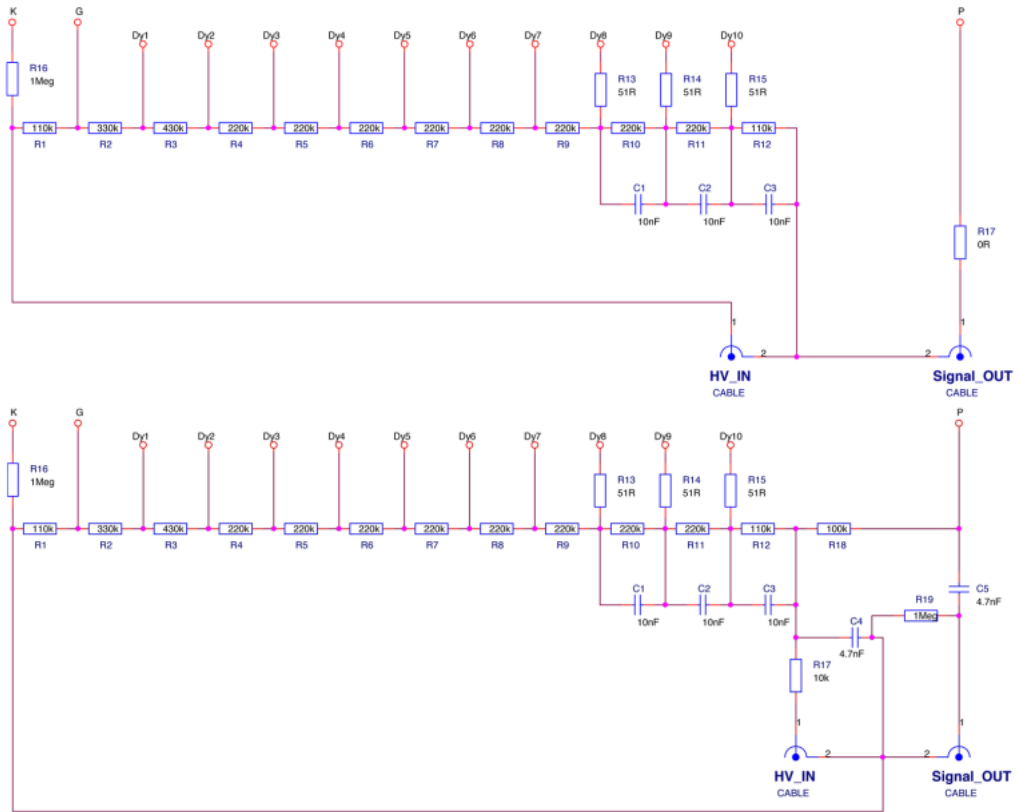


**Figura 2.9** – Hamamatsu commercial voltage divider electronic circuit. Upper circuit with negative supply and lower circuit with positive supply. [62]

other circuit, supplied with positive voltage, can be interesting for other tasks such as measurement of PMT currents. We will use both, depends on the objective of the study.

Focusing electrodes are used to get the photoelectrons to reach the first dinode. Therefore, they have an collection efficiency (CE) that is defined as the quotient between the number of photoelectrons reaching the first dinode and the number of photoelectrons leaving the photocathode and whose value is around 80% for PMTs.

The dynodes is the part where the multiplication takes place. They have different voltage between each dynode in order to accelerate the electrons sufficiently so that, when the electron hit the each dynode, several electrons are emitted. The multiplication factor,  $\delta$ , is the multiplication of electrons in each dinode and its value is commonly around 5 and it has a strongly dependence with the HV. If we take into account that the PMT has N dynodes, commonly N=10 and we guess that each dynode has de the same gain,  $\delta$ , the overall gain of the PMT is:

$$G = CE \cdot \delta^N \quad [55] \quad (2.8)$$

If we use the numerical values mentioned in this section, we can see that the overall gain of a general PMT will be of the order of  $10^6$ . It is important to mention that this value depend strongly on the HV used.

We have to take into account that the uncertainty of the output signal with this gain is much greater than without it. That is the reason why, there are some times that it is interesting to work without gain such as when we try to count the number of photons that reach our PMT. We can achieve it with a small modification of the electronic voltage divider circuit 2.9. It consists of short-circuiting all the dindes and the anode. In this way we are collecting the signal in the photocatode in

which no amplification has occurred. We will use this voltage divider circuit without gain in our study with fibers.

Finally, when the amplification is used, the anode is the point where the collection of all the electrons produced in this multiplication process takes place and it is the one that gives rise to the output signal of PMTs.

Due to the fact that all intermediate factors (photoelectric effect and multiplication of electrons) are linear, the output signal of a PMT will be linear with the number of photons that reach its sensitive part. It will occur until a large number of photons reach the photocathode at the same time, where saturation will occur and linearity will be lost. This limit depend on the specifically PMT which we are using. This output signal has a spread of the order of tens of nanoseconds.

The multiplication of electrons can be described as a Poisson statistical process, so, for each electron in the first dinode, we will have  $G$  new electrons whose variance will be approximately  $\sqrt{G}$ .

Finally, we have to take into account that the photocathode can emit electrons whose origin doesn't belong to the scintillation light. This signal, which is named dark current, can happen due to several reasons like cosmic radiation, light from environment or thermoionic emission (the dominant) and, for our PMTs, this value will be around 2 nA according to Hammamatsu data sheet.

The calibration of the most important parameters (for our objective) of the PMTs used, which are dark current, gain for several HV and quantum efficiency, have been done at IFIC in the framework of NEXT experiment [61].

### Silicon Photoelectron Multiplier Array (SiPMs array)

The Silicon Photomultiplier (SiPM) is a photosensor, based on semiconductor materials, which has been developed in recent decades and they are replacing conventional PMTs in some experiments or applications. They have been designed to archive outstanding photon-counting capabilities better than conventional PMTs with high gain and high photodetection efficiency equal to or larger than conventional PMTs but with some important differences like insensitiveness to magnetic fields, low operating voltage, compactness among other differences.

### Semiconductor materials

Silicon is a semiconductor material and, like any semiconductor material, it has an electronic band structure that consists of two bands: Valence band and conduction band which are separated by a forbidden energy gap (with width of around 1 eV for semiconductors [56]) where there cannot be electrons. These energy bands are based on many energy levels that are so close that we can consider a continuum. You can see a diagram of these bands in Figure 2.10.

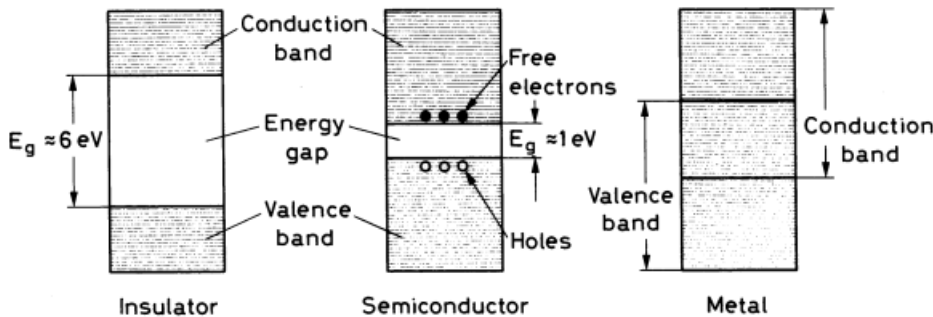


**Figura 2.10** – Energy band scheme for (a) insulator, (b) semiconductor and (c) conductor. [56]

Electrons in the conduction band, unlike those in the Valence band, can move freely in the material so they contribute to the electric current.

Silicon has four electrons in their valence band (tetravalent atom) so it forms four covalent bonds creating a crystal lattice ( $\text{Si}_2$ ). Normally a small quantity of impurities ( $10^{13}$  atoms/ $\text{cm}^3$ ) are added to modify this lattice, that's doping the material.

If the dopant has 5 valence electrons (pentavalent atom like phosphorus or arsenic) there will be a free electron which will be at an energy level created in the forbidden band, very close to the conduction band. It is called "n-type" semiconductor and the electrons are the majority charge carriers.

Otherwise, if the dopant has 3 valence atoms (trivalent atom like gallium or boron) it will have a hole<sup>5</sup> that will be at an energy level created in the forbidden band, very close to the valence band. In this case, the holes are the major charge carriers and this element is called "p-type" semiconductor.

Both configurations (p-type or n-type semiconductor) are shown in the figure 2.11.

SiPM is based on a silicon diode formed by a junction of n-type and p-type semiconductors that is made with special techniques to achieve a good contact between both surfaces.

This union creates the so-called depletion zone, which is the interface between both materials. In this zone, there is a diffusion of electrons to the p-type semiconductor and holes to the n-type semiconductor due to the difference in the concentration of the majority charge. This re-arrangement of the charge creates an electric field in the depletion zone contrary to the movement of these charges, whose potential difference, called contact potential, is  $V_0 = 0.7 \text{ V}$  for silicon [56]. All this information is shown schematically in the figure 2.12

There are no charge carriers in the depletion zone and, if any one

---

<sup>5</sup>Electron absence in the crystal lattice

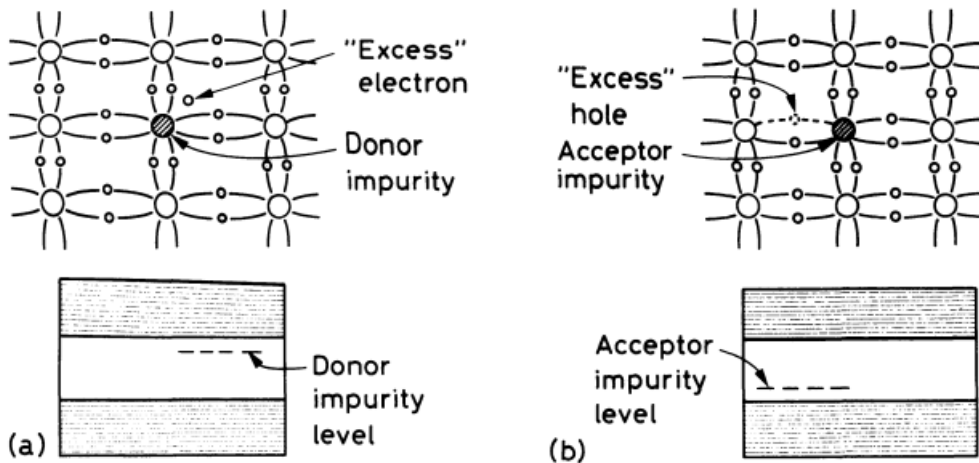


**Figura 2.11** – Crystal lattice and energy band scheme formed by a silicon with (left) a pentavalent dopant that creates an n-type semiconductor (right) a trivalent dopant that creates a p-type semiconductor. [56]

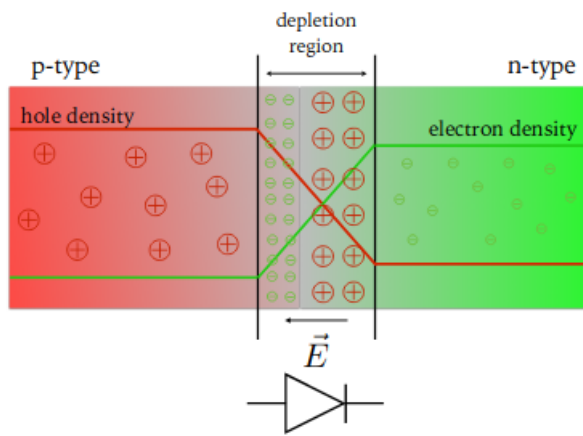


**Figura 2.12** – (Above) Schematic of the charge distribution and electric field created in a pn-junction. (Bottom) Commonly used symbol for a diode. [63]

are created, they will be swept out by the electronic field (special interesting property for radiation detectors since charge carriers are created in this zone when ionizing radiation crosses through it).

If we want to use this p-n junction as a particle detector, this setup has some problems that we have to overcome. On the one hand we need to prevent the charge recombination in order to optimize its collection in the depletion zone. On the other hand we need to increase the width of the depletion zone (it is  $0.5 \mu\text{m}$ , too small to stop interesting particles) and, as we will see in the section 3.3, this small width increases the capacitance value that will increase the noise in the output signal.

We managed to overcome these problems if we apply a bias voltage across the junction. If this bias voltage is with positive terminal in p-type semiconductor and negative terminal in n-type semiconductor, which is called forward bias voltage, it will create an additional electric field opposite the internal electric field, which will attract electrons in n-type towards p-type and holes in p-type towards n-type. In short, it will reduce the depletion zone, and if the applied voltage is greater than the contact potential, an electric current will be created even if no charge has deposited their energy in the depletion zone.

However, if this bias voltage is applied with positive terminal in n-type semiconductor, negative terminal in p-type semiconductor, which is called reverse bias voltage, the contrary effect will happen and the intensity of the electric field in the depletion zone will be increased. This effect will be limited by the resistance of the semiconductor and if we use a too large bias voltage the pn-junction will breakdown and it will begin conducting.

If reverse bias voltage is applied, we can solve all the problems mentioned above. In this case, the charge collection will be improved and the width of the depletion zone will be increased. If ionizing radiation crosses the depletion zone, which is wide enough to detect interesting particles, it

will deposit their energy and, due to that, charge carriers will be created<sup>6</sup> which will be swept due to the electric field and an optimized current signal will be created.

Depending on the intensity of the polarization voltage we can work in different modes and we will have different output signals. If the bias voltage is less than the threshold, the charge carriers will recombine and no output signal will be produced. If the bias voltage is larger than threshold an avalanche is created due to each original electron and it is independent of other possible avalanches. Due to this avalanche, it has a gain whose value is around 200. This mode is called proportional mode since the collected charge is proportional to the energy deposited. Finally, If the bias voltage is even larger, each avalanche can trigger a second avalanche and, due to that, their internal gain is higher than the proportional mode<sup>7</sup>, that's, its output signal will be larger. This mode is called Geiger mode since the output signal only shows when a detection has happened but it is not proportional to the energy deposited.

The voltage at which the SiPM changes from proportional to geiger mode is called the breakdown voltage,  $V_{BR}$ . If it works at a lower voltage it is in proportional mode but if it works at a higher voltage, it works in geiger mode. The measurement of the breakdown voltage is one of the most important things to characterize the SiPM and I show how we have done it in the section 3.3.

### Silicon photomultiplier

The SiPM is based on a matrix of APDs which are photodiodes operating in geiger mode. A scheme of an APD used in a SiPM is shown in the figure 2.13. It has p+ and a n+ layers<sup>8</sup> that are used because they

<sup>6</sup>The energy required to create an electron-hole pair in silicon is 3.62 eV in STP[56]

<sup>7</sup>The gain of commercial SiPMs, for example Hammamatsu, is of the order of  $10^6$ , similar to the PMTs

<sup>8</sup>p+ and n+ layers are the same as p and n layers, explained before, but with higher

improve the properties of SiPMs but the way these APDs work is the same as that described before.

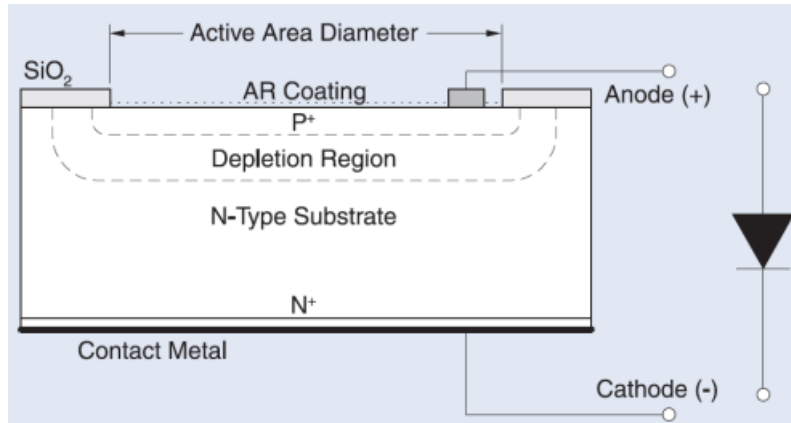


**Figura 2.13** – Scheme of a APD and electrical symbol used. [64]

These APDs, called pixels when they are part of a SiPM, are connected in parallel and we read the sum of all of them at each moment. The output signal of each pixel is approximately the same regardless of the energy deposited, with some difference due to the uncertainty in the SiPM manufacturing process and the statistical nature of the detection process. Due to that, we cannot know the energy deposited in each APD but, as we read all SiPM pixels at the same time, as you can see in the figure ??, the charge on the output signal when we detect  $n$  photons simultaneously will be  $n$  times the charge we have when we detect only one photon. Due to this property, after a correct calibration of our SiPMs which will be shown in the section 3.3, we can know how many particles (photons in our case) we have detected, which have a linear relationship with the output signal.

Furthermore, as we saw in section 2.2.2, since we work with scintillators, in our case, the number of photons is proportional to the deposited energy, so we can recover the characteristic linearity of its output signal and to know the energy deposited in our scintillator, and, therefore, the energy concentrations of acceptor impurities or donor impurities respectively CHECK THAT!!

of the initial radioactive event, which will be one of the most important parameters in our signal.

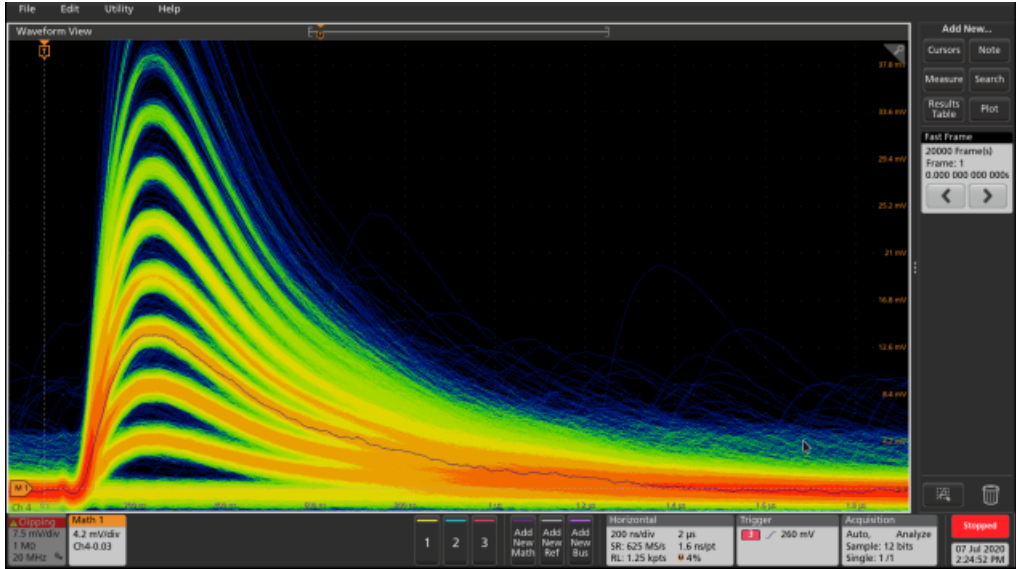


**Figura 2.14** – Using persistence on the oscilloscope to show several pulses with different heights. Each height associated with a different number of SiPM pixels lit at the same time.

On top of that, these pixels need to be so small<sup>9</sup> that, if the photon density to be detected is low enough, we only detect one photon in each pixel. If it doesn't happen, we will detect two or more photons with the same pixel but the output signal will be the same as one detected photon, so we will have a loss of linearity of our output signal. This effect is known as saturation and it is important to know the photon density at which it happens for our SiPMs. The experimental measurements of this effect, which have been done for our SiPMs, is shown in the section 3.3. SI LA MIDO YO PERFECTO, SI NO PONER UNA FOTO DE LA TESIS LARGA.

Each of these pixels has a quenching resistance<sup>10</sup> in series that is

<sup>9</sup>Pixel sizes for commercial SiPMs are 50 or 75μm [65], [66]

<sup>10</sup>The typical value of this quenching resistance for commercial SiPMs is around 500 kΩ

used to stop the current produced when this pixel has detected a particle. It is used for limit the current drawn by the diode during breakdown and reduce the reverse voltage seen by the diode to one below the breakdown voltage. After that, the voltage seen by the diode is reset to the bias voltage and this pixel is ready to detect a new particle again. In figure 2.15 (left) a diagram of these chenching resistances and APDs in a SiPM and (right) how it works is shown respectively.

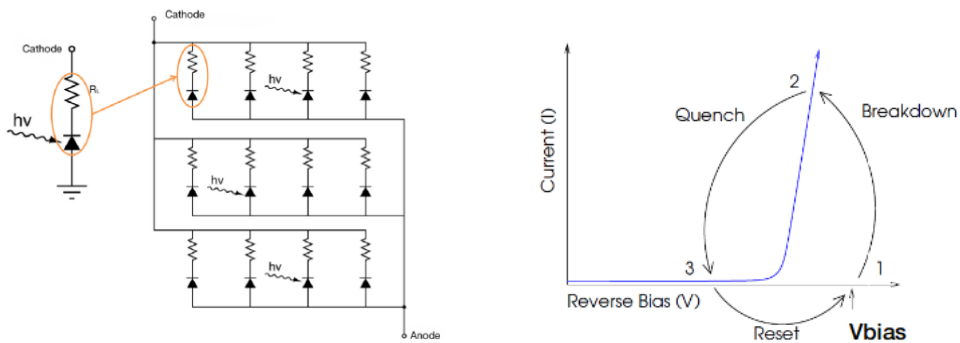


**Figura 2.15** – (Left) Electronic scheme of a SiPM and (right) output current of a SiPM as a function of the reverse voltage. It show that the quenching mechanism is essential for working with SiPMs [69]

In this simple electrical scheme we can see that all pixels have a common cathode and anode which means that, as we said before, they are at the same bias voltage and the output is the sum of all of them.

We have a lot of names to refer to these photosensors such as SiPMs, MPPCs, G-APDs, SSPMs, MRS-ADPs or AMPDs. The candidate for TRITIUM project is S13360-6075 from Hamamatsu photonics [66] because its characteristics are the ones that best fit our objectives since this model has super low afterpulses, crosstalk and dark counts than other SiPM models from Hammamatsu. Its characteristics and properties are shown in the table 2.3.

These characteristics and properties will be explained and their

Parameter	Numerical value
Serie	S13360
Model	6075
Pixel Pitch ( $\mu\text{m}$ )	75
Effective photosensitive area ( $\text{mm}^2$ )	$6.0 \times 6.0$
Number of pixels	6400
Fill factor	82%
Refractive index of windows material	1.55
Operating temperature range ( $^\circ\text{C}$ )	[−20, 60]
Spectral response range, $\lambda$ (nm)	[320, 900]
Peak sensitivity wavelength, $\lambda_p$ (nm)	450
PhotoDetection Efficiency, PDE, $\lambda = \lambda_p$ (%)	50
Dark counts, Typical/Maximum (kcps)	2000/6000
Terminal capacitance, $C_t$ (pF)	1280
Gain, M,	$4 \cdot 10^6$
Breakdown Voltage, $V_{BR}$ (V)	53
Cross talk probability(%)	7
Temperature coefficient $\Delta TV_{op}$ (mV/ $^\circ\text{C}$ )	54

Table 2.3: Characteristics of SiPM S13360-6075 from Hammamatsu Photonics [66].

experimental measurements will be shown in section 3.3. These numerical values, which appear in the table 2.3, are provided by Hammamatsu photonics but it is only an approximation for this model. These parameters must be determined experimentally for each SiPM used because it can be very different even if it is the same model.

It must be taken into account that we will do this characterization at the level of a single SiPM because, at the beginning, it is easier to understand the results but we will work with a matrix of them and we will have to do this characterization for each matrix used.

The matrices under consideration are the model "S13361-6050" from Hammamatsu, which consists of a  $4 \times 4$  SiPM matrix where the active area of each SiPM is  $6 \times 6$  mm [67] or the model "S13361-3050" from Hammamatsu, which consists of a  $8 \times 8$  SiPM where the active area of each is  $3 \times 3$  mm [68]. They are a commercial matrices from Hammamatsu and, as you can see, the total active area that we will cover with these arrangements is the same in both cases,  $24 \times 24$  mm and it is approximately the same that the active area covered with the PMTs used, which has been shown in the previous section.

These matrices have a common bias voltage and common ground for all SiPMs that are contained and we will have an output signal for each SiPM.

We hope to obtain better results with the  $4 \times 4$  matrix for theoretical reasons which we will see in the section 3.3 like larger PDE, mainly due to a larger active area but it is something that we will have to verify with experimental measurements.

Nuestro SiPM esta dopado? con que?

### Comparison of photosensors considered

As we have said before, we are going to use two of the most widely used photosensors in the world, PMT and SiPM. Each has some properties that are better than the other for our experiment and its own problems. We will have to test both and choose the one with which we achieve better results.

The output signal of both photosensors used is proportional to the number of incident photons and they have a similar internal gain (of the order of  $10^6$ ). Both properties are essential for our experiment in order to detect tritium events and obtain a signal large enough to be measured and processed.

They have fast output signals, whose rise time is shorter than nanoseconds, and a wide spectral sensitivity that is similar for both ([200 – 800] ns for PMT and [300 – 900] ns for SiPM).

The supply voltage necessary to work with SiPM, on the order of tens of volts, is much lower than that of PMTs, which require high voltage, that is, on the order of thousands of volts and the PDE at 420 nm, achieved with SiPM is higher, around 50%, than PMT, whose PDE is around 30%. A large PDE is essential because, as we have seen before, the number of photons that we will read in each tritium event will be very low, so we must detect as many photons in each event as we can.

Furthermore PMTs, due to the reason that they consist of a vacuum tube, are more bulky and fragile than SiPMs, which are compactness and robust. It is an advantage of the SiPMs because we want that our detector work during a lot of years so we need this to be durable. Furthermore, because PMTs are manually produced, they are much more expensive, thousands of euros, than SiPMs, tens of euros, which can be mass produced.

On top of that the behavior of the PMTs is affected by magnetic fields, something which doesn't happen with SiPMs with which it has been

tested that it can work correctly with magnetic field intensities between 0 and 7 Tesla.

In addition to that, due to their enormous uniformity, SiPMs are capable of distinguishing the exact number of photoelectrons detected and even resolving a spectrum of a single photoelectron, which is not possible with PMTs due to variations in their gain.

On the other hand, the dark current rate for PMTs is much lower (a few counts per second) than for SiPMs, whose dark current rate is between 0.1 and 1 Mcps<sup>11</sup> (depends on its size) and it happens almost entirely at the level of a single photoelectron. It is a problem of the SiPMs because we need to distinguish the tritium signal from this background. In addition to that, SiPMs have other properties, such as the crosstalk of the afterpulses, that must be measured and extracted since they can affect the correct measurement. We will see how to do it in the section 3.3

Also, the SiPMs output signal is affected by a slight change in temperature, something which doesn't happen with PMTs. It is a serious problem of the SiPMs for our experiment because we will work in the field, where we cannot avoid such a low temperature change. As we will see in section 3.3 we will solve this problem with a suitable change in the supply voltage that compensates for this variation.

---

<sup>11</sup>Mega counts per second,  $10^6$ c/s

## 2.2.4 Readout system of photosensors

The last part we need to have a complete scintillator detector is the electronic system that is the part in charge of reading, processing and analyzing the output signal of the photosensor used and providing us with information that we can interpret.

This electronic system will depends on the type of the output signal of our detector. Therefore, it will be different for the different detector configurations that has been tested in our experiment. It includes PMT and SiPMs and these will be the parts in which this section is divided.

### Electronical system for PMTs

In the different tests in which we have used PMT, we were interested in two different main objectives. On the one hand, we were interested in knowing the amount of incident photons that reached the PMT photocathode, which can be interesting, for example, to characterize fibers, and, on the other hand, we were interested in the energy of each event that occurred, which can be interesting, for instance, to obtain an energy spectrum or to discriminate events based on their energy (for knowing the origin of these events and counting only interesting events).

In the first case, if we want to know how many photons have reached the photocathode, we have to work without the internal gain of the PMT. The reason for this is that it introduces a large uncertainty in the measurement. The use of this internal gain could be interesting in other situations such as when we need to know the energy of the event because, as we saw in the section 2.2.3, its use greatly enlarges our signal, a factor of the order of  $10^6$ , and, due to that, it is easier to process and analyze it.

For working without the internal gain of the PMT we need to avoid

the use of the electron multiplication stage that we saw in section 2.2.3. To achieve this, we design, build and test special PCBs, whose electronic scheme is shown in figure ??, in which we short-circuit all the dindes and read the signal directly from the photocathode.

### PHOTO AND ELECTRONIC DESIGN.

This PCB is designed to be powered with positive supply voltage which is less than the normal situation [0 – 400 V]. The reason of this lower supply voltage is that we don't need to create a voltage difference between each pair of dynodes in the chain (we only need to create a voltage difference between the photocathode and the first dinode).

In this case, the output signal of our photosensor is very fast and small (currents of the order of tens of nanoamperes<sup>12</sup>) and we need a special system to analyze these types of currents. The system which we have chosen is Keithley 6487 Picoammeter/Voltage Source [70], which is a commercial system from the Keithley company, because it has some interesting options for this study such as automatic baseline correction, the ability to read signals as small as picoamps and the ability to perform some interesting mathematical operation, such as the average of N measurements with the associated statistical error, where N is programmable by the user ( $N = 100$  in all our studies).

With this configuration we can measure the output current of our photosensors and, from it, quantify how many photons have been detected by the PMT photocathode using the equation 2.9:

$$N^o \gamma / \text{sec} = \frac{(I_{PMT} - I_{DC})}{q_e \cdot QE \cdot CE} \quad (2.9)$$

Where  $I_{PMT}$  is the output current of the PMT when it detects

---

<sup>12</sup>1 A =  $10^9$  nA

photons and  $I_{DC}$  is the dark current of the PMT. This equation takes into account the quantum efficiency, which is close to 30% for the PMTs used, and the capture efficiency in the dyndes, which is equal to 1 because we read the signal directly from the photocathode. In addition, it is taken into account that, due to the photoelectric effect in which this detection consists, each detected photon only generates one electron, whose charge is  $q_e$ .

In the second case, if we want to know the energy of the event that occurred, we need to work with the internal gain of the PMT. For that we will use the electron multiplication stage that we saw in section 2.2.3.

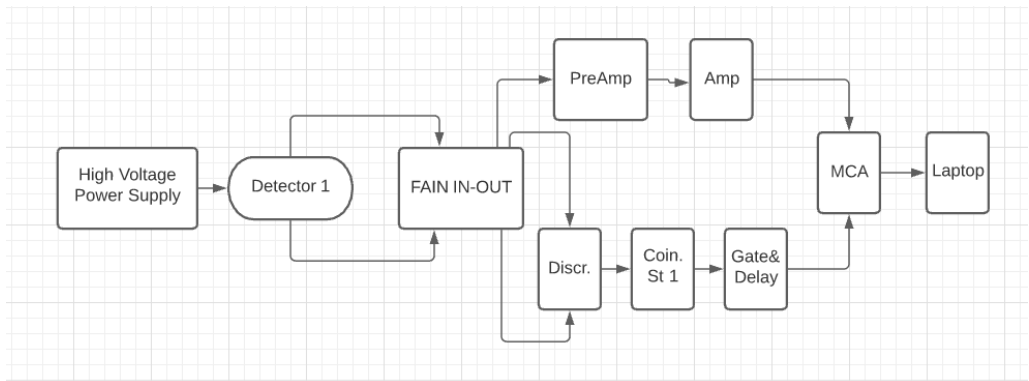
In all our studies we have used several PMTs in our experiments (two or four depend on the case). The electronic schematics used, which are shown in figure 2.16a and 2.16a respectively, are based on various NIM technology modules<sup>13</sup>.

The PMTs used in each situation are feeded with the voltage supply "TC 952 High Voltage Supply" from Tennelec [71]. It has four channels for feeding up to four different PMTs so it is enough for both configurations. In some situations we need to work with both configurations at the same time, that's, with six PMTs at the same time. In this cases other voltage supply had been used, called "HV Power Supply N 1130-4" from "Wenzel Elektronik" [72] company with which we get 4 additional channels for feeding PMTs. The high voltage used in each case will be named in each specific situation.

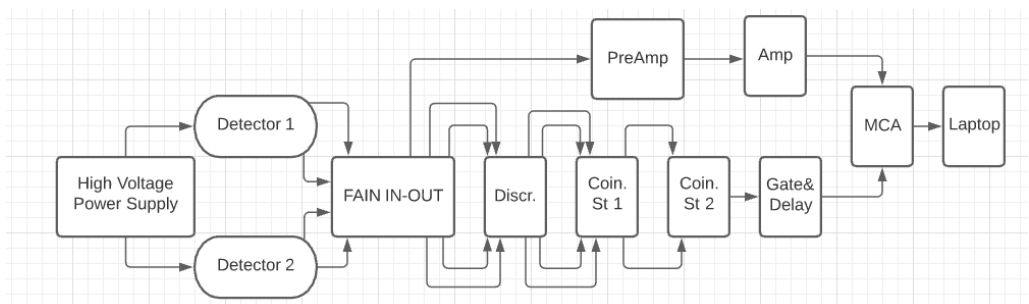
As you can see in the figures 2.16a and 2.16a, in both electronic configurations there are two different paths that must be followed by the output signals of each PMT, the amplification part and the time coincidence part. Therefore, the first module we need is the analogic FAN IN-OUT module which is used to duplicate the input signal.

---

<sup>13</sup>The Nuclear Instrumentation Module (NIM) is a standard specification convention for electrical and mechanical parameters defined in electronic modules used in experimental nuclear and particle physics.



(a) Electronical configuraition scheme used to measure with two PMTs.



(b) Electronical configuraition scheme used to measure with four PMTs.

**Figura 2.16** – Schemes of different electronic configuration used to measure with PMT.

The module used is the "Quad linear FAN IN-OUT MODEL 740" module from the company "Philips Scintific" [73]. With this module we can obtain up to 4 output signals (we only need two) that are totally identical to each input signal. For each PMT we have two identical output signals. One will be used as the input for the amplification part and the other will be used as the input for the time coincidence part.

- The amplification part, which is the same for both electronic configurations, figures 2.16a and 2.16b, is used to process and amplify the output signal and it is the same for both configurations. We have to take into account that we have only used the signal from one PMT for the amplification part. We could have added a stage where we add the four PMT output signals and it would probably improve our results, but since our ultimate goal is to work with SiPM, we have not delved into that.

The electronic path we have followed to achieve this amplification is:

1. In this part we introduce one of the output signals of the previous module (FAN IN-OUT) in a preamplifier that is used to prepare the signal to be amplified, appendix B. The preamplifier used is "MODEL 9326 FAST PREAMP" from ORTEC [74].
  2. The output signal from the preamplifier is introduced into the amplifier where it will be converted to a positive signal with a shape close to the Gaussian function and an amplification factor will be applied. The amplifier modules used on this studies are "model 575A" and "model 671", both from ORTEC company [75], [76]. The output signal for 575A module is shown in figure 2.18, green color.
- The time coincidence part is used to obtain the coincidence gate that will be used to indicate when we have to save the amplified signal

(which is when all the PMT output signals are in time coincidence). Only the saved output signal will be used for the analysis.

This part is practically the same in both cases with just one additional step when we use four PMTs. The electronic path followed in the time coincidence part is:

1. The second output signals of the FAN IN-OUT module for each PMT are introduced into a discriminator module where we obtain an output logic signal with height of  $-1.2$  V and width of 240 ns when a threshold, the one programmed by the user, is exceeded. The discriminators used in our experiments are "Octuple Constant-Fraction Discriminator CF8000" module from ORTEC company [77] and "4 channels discriminator model 84" from CAEN company. These four output signals are shown in figure 2.17d for four PMTs in coincidence.
2. Now is the time to make time coincidences. As we will see in the section 2.4.2 and chapter 4, we have two photosensors in each detector, so we will do time coincidences in pairs of photosensors, PMTs in this case.

Therefore, each pair of output logic signals of the discriminator module (attached to two PMTs that are in the same detector) will reach a different channel of the coincidence module and generate an output signal, with a height of  $-1.4$  V and width of 20 ns, when a time coincidence has occurred on them.

This first time coincidence stage is used to remove the detection of external light or dark current of PMTs from in the saved measurements. This is because this module only generate logic output signals when both PMTs have detected photons at the same time, indicating that these photons are coming from the coupled scintillator.

The time coincidence modules used are "Coincidence Unit Model

465" from LeCroy [79] and "Coincidence Type N6234" from CERN-NP [?].

3. The next step, which is included only when working with four different PMTs, is used to do time coincidence between two different detectors. It could be interesting, for example, to detect hard cosmic radiation as we will be in the 2.4.2 section.

If we want to do time coincidences between both detectors, we have to use the logical output signals of the previous step (output of the coincidence module) as input of another coincidence stage similar to the previous one. In this case, which is only used when we have four PMTs, we will have a logical output signal with the same parameters, height of  $-1.4$  V and width of 20 ns when both detectors have detected events at the same time. The modules used is the same named in the previous point.

In the figure 2.17 we have shown all the different situations that we can have with the previous two steps. There we have four logical signals from four PMTs. The two first signals (channel one and two) come from two PMTs connected to one detector and the other two signals (channels three and four) come from PMTs connected to another detector.

- (a) In figure 2.17a we can see that only one PMT (channel two) has detected an event. As the second PMT connected to the same detector (channel one) did not detect this event, it indicates that the detected photons did not come from the scintillator. In this case, the time windows (output from coincidence module, stage 1) will not be opened and this event will not be saved.
- (b) In figures 2.17b and 2.17c we can see that two PMT signals connected to the same detector have detected an event but the others have not. It means that it is an event that has only been detected by one detector. If we are using the second stage of time coincidence, the time window will not open to

save this event.

- (c) In figure 2.17d we can see that, in this case, all signals have detected the event. It means that it is an event that has been detected for both detectors. In this case, a time window will be created to save this event.

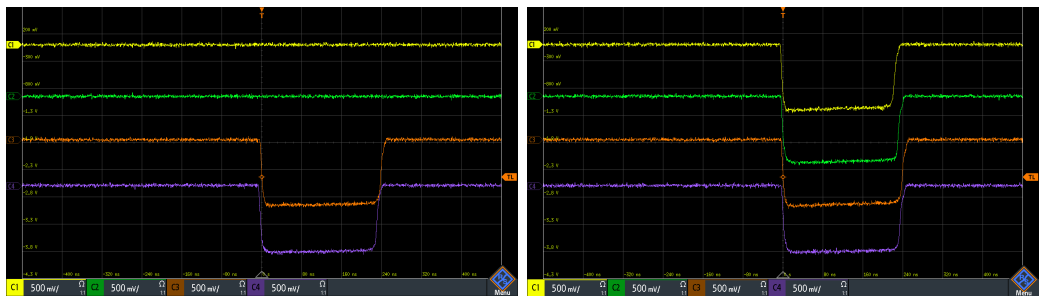
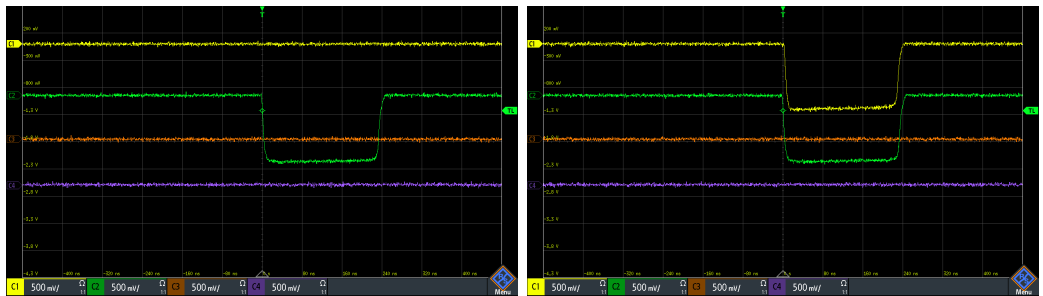


**Figura 2.17** – Different situation that can happen when we do time coincidences with PMTs.

4. Finally, the logical output signal of the coincidence module used, which indicates that all the PMTs used in our study are in temporal coincidence, is introduced in the "Gate and Delay Generator, model 416A" of the company ORTEC [80]. With this NIM module we obtain a positive logical signal, shown in the figure 2.18, orange color, with a height of 8 V and width of 2  $\mu$ s.

At the end, we have two different signals, shown in figure 2.18, which will be introduced in the MCA 8000D, Pocket MCA from AMPTEK company [81] to be saved. On the one hand we have an analog signal (output from the amplifier module) that has information about the event that has been detected (its energy, detection time, etc.) and this is the signal whose information we will save for analyzing. On the other hand we have a logic signal (output from the Gate and Delay Generator module) that indicates when we have to save the amplified signal, that is, when all our PMTs used in our experiment have detected an event at the same time.



**Figura 2.18** – Signal amplificated and logical gate (input signals of MCA).

The information that will be saved and histogrammed in the MCA is the weight of the signal, which is proportional to the energy of the detected event, explained in the appendix B. An example of histogram as output of the MCA is shown in figure 2.19.

**Figura 2.19** – Energy spectrum obtained with the electronic configuration explained in this section for four PMTs.

### Electronical system for SiPMs

Before talking about the electronic system that is used for reading SiPM, we have to keep in mind that we are using SiPM arrays in TRITIUM detector. The electronic system used to process and analyze these output signals is PETSYS [82], which is a commercial system prepared to work with SiPM matrices from Hammamatsu, which is the SiPM company chosen for us.

Petsys system, figure 2.20, is a complete acquisition and digitization system that is capable of working with up to 1024 SiPM arranged in matrices of up to 64 SiPM per matrix. This capacity is necessary because, as we will see in chapter 4, TRITIUM monitor will use dozens of SiPM matrices with 16 channels (SiPMs) per matrix.

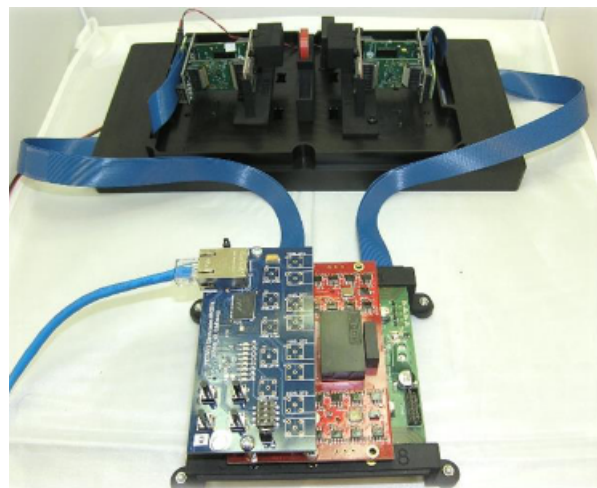


**Figura 2.20** – Different parts of PETSYS system. [82]

Taking into account the current detection limits imposed, this capacity should be enough for TRITIUM detector but, as we will see in chapter 4, TRITIUM is a modular detector. If we need to overcome its limits reached (improve its sensitivity or reduce their background even more) we will need to increase this capacity. We need an electronic system that is

able to increase its capacity in a modular way and PETSYS meets this requirement. It has the Clock and Trigger module with which we have the possibility of connecting up to sixteen different PETSYS basic boards in parallel with which we could read up to 16384 SiPM<sup>14</sup>.

PETSYS is based on C++ and Python scripts that are prepared for the main tasks required for our experiment, such as time coincidence options between SiPM (or even SiPM matrices) or energy discrimination. In addition, PETSYS is open source, so if it is necessary, we have the option to modify the scripts for developing interesting functions. The way the signals will be processed and analyzed for PETSYS will be exactly the same as those shown in the figure 2.16

This system has a time resolution of 250 ps which is one of the best time resolutions of commercial systems available today and its price is around 10€/ channel, which is very cheap in comparison with current similar electronic systems.

As we will see in the section 3.3, the temperature of each SiPM matrix is an important parameter to take into account. The PETSYS system has the ability to monitor the temperature of both, the SiPM matrices and ASICS that are used to control them during the measurements.

Although PETSYS is the system used to work with SiPM matrices in the TRITIUM detector, it does not allow characterizing the SiPMs, which is an important task to understand the results of our detector.

In order to do so, we have designed, developed and built an electronic system with which we can read up to eight different SiPMs. With this system we can also monitor the temperature of the SiPMs used.

This system is based on three different PCBs<sup>15</sup>, which are shown

---

<sup>14</sup> $1024 \cdot 16 = 16384$

<sup>15</sup>PCB, Printed Circuit Board

in figure 2.21 and whose electronical schemes are shown in the appendix C:

1. The first PCB, shown in figure 2.21a, is used to organize the SiPMs and sensor temperature in this system. This PCB has the ability to place up to 8 different SiPMs and a temperature sensor and arrange these signals on two HDMI connections.

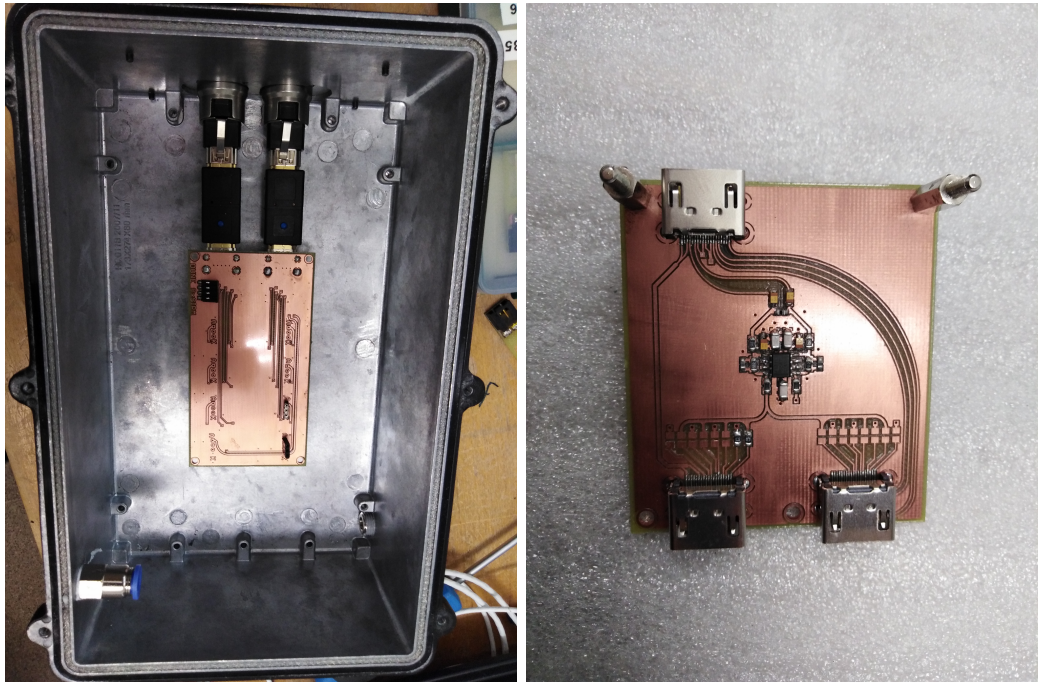
This PCB will be inside a special black box, from "" company, that has a high degree of light tightness. This black box has a small hole, whose diameter is 1 mm, prepared to introduce an optical fiber<sup>16</sup> with which we will illuminate the SiPM with a incoherent light source. The light source used is a LED, "" from the "" company [], whose emission spectrum is shown in the figure 2.21d. With this LED we try to simulate the output signal of the fibers used in our experiment.

2. The second PCB, shown in figure 2.21b, is used to sum the different signals from the SiPMs used in the first PCB and amplify the output signal by a factor G. This PCB uses a differential amplification with which we achieve to reduce the electronic noise of the system.
3. The third PCB, shown in figure 2.21c, is used to arrange all the different input and output signals of this system in an HDMI connection with which we connect to the second PCB. The objective of this PCB is to avoid the introduction of electrical noise by crosstalk between different signals.

The input signals of this system are the supply voltage of the SiPMs and the supply voltage of the PCBs ( $\pm 6$  V) and the output signals of this system are the temperature sensor signal and the summed signal of all SiPMs.

---

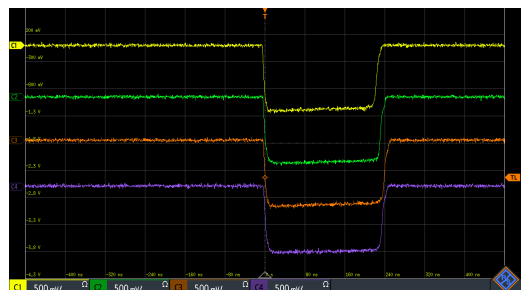
<sup>16</sup>The optical fibers used are BCF-98 from Saint Gobain company [83]



(a) PCB 1 used to arrange 8 SiPMs and black (b) PCB 2 used to sum and amplify the output signals of SiPMs



(c) PCB 3 used to arrange the different signals of the system.



(d) Emission spectrum of the LED.

**Figura 2.21** – Three PCBs used for the SiPM characterization and LED emission spectrum.

## 2.3 Ultrapure water system

### 2.3.1 Introduction to the ultrapure water system

The aim of using an ultrapure water system is to condition the sample before the measurement. It is important for two reasons:

- On the one hand, it is important because, as we saw in section 1.2, the mean free path of tritium electrons in water (our case) is around  $5 \mu\text{m}$  and even less for solid materials like organic material.

For detecting this tritium decay, we need that the electron of its decay reaches the fiber, so we must keep our detector clean. If the analyzed water sample contains particles that can be deposited on the fibers of our detector, it can form a layer of matter, which prevents the tritium electrons from reaching the fibers, reducing the tritium detection efficiency until it becomes impossible to measure tritium.

- On the other hand, we have to keep in mind that, as we will see in chapter 4, the tritium monitor does not have any spectrometric capabilities that can be used to distinguish other radioactive elements from tritium. That means that, all the radioactive element included in the analyzed water sample will be computed as a tritium event.

With this system we can remove all particles up to a diameter of  $1 \mu\text{m}$  and organic matter, which means that we remove all particles and molecules other than water. Since tritium is the only radioactive element that can be practically equal to water (when it is in the HTO form, the majority form in which tritium are present in the water sample), with this process we remove all particles radioactive elements other than tritium and the amount of tritium present in the sample is not affected

In summary, with the ultrapure water system we get to keep our detector clean, ensuring the stability of its detection efficiency and we eliminate all radioactive particles other than tritium, maintaining the activity of the tritium in the sample, so we do not need any spectroscopic capabilities in our detector to distinguish radioactive elements. Both reasons has been tested with experimental measurements that will be shown in the chapter 3.4.

### 2.3.2 Set up of ultrapure water system

The main objectives of this water treatment device are:

- Obtaining a high degree of purification in the processed water sample, reducing its conductivity by approximately two orders of magnitude (from  $1000 \mu\text{S}/\text{cm}$  up to  $10 \mu\text{S}/\text{cm}$ )
- Designing of a device with low maintenance (low cost and low man-power)
- Installation of a remote control devices such as probes and valves and development of a software to management it.

For this, the LARUEX laboratory in Extremadura, one of the six collaborators of the TRITIUM experiment, has designed, developed and built an ultrapure water system, whose scheme is shown in figure 2.22.

This system has been installed in the Arrocampo dam and consists of four different consecutive stages:

- First, the raw water from the Tagus River is introduced into two different filters, the first formed by Silex-Anthracite and the second

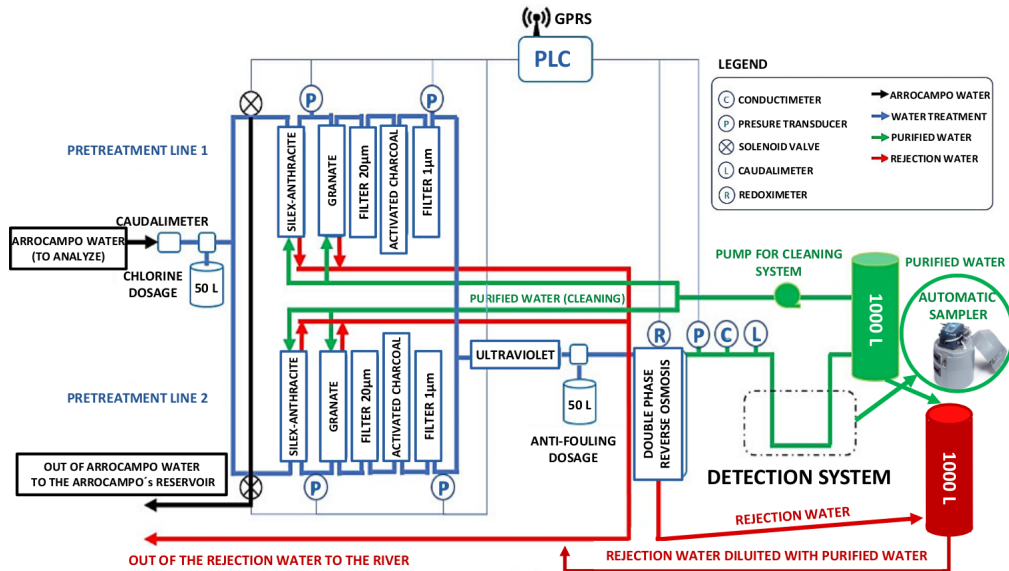


**Figura 2.22** – Scheme of water purification system.

by granate, with which we make a gross filtering (the largest particles are eliminated). There are two parallel lines that are capable of self-cleaning by injecting ultrapure water in the opposite direction.

- Next, this water sample is introduced into a  $20 \mu\text{m}$  filter (Formed by a synthetic mesh) and activated charcoal filters (one per line in both) that form the fine filtration stage. With the  $20 \mu\text{m}$  filter we can filter particles with diameters of up to  $20\mu\text{m}$  and, with the activated charcoal filter, we remove the chlorine and iron particles from the sample.
- Then, this water sample is introduced into the super-fine filtering consisting of a  $1 \mu\text{m}$  filter, formed of a dense polypropylene mesh, (one per line), and UV lamps. With the first we remove all the particles up to diameters of  $1 \mu\text{m}$  and, with the second, we remove the organic matter present in the purified water sample.
- Finally, this water sample is introduced in the last stage, double-

phase reverse osmosis, thereby reducing the conductivity of the water to values of  $5 \mu\text{S}/\text{cm}$ . We verified that we achieve a conductivity of  $10 \mu\text{S}/\text{cm}$  with only one module reverse osmosis and this is enough for the needed conditions of tritium detector. Therefore, we use just one module of reverse osmosis for 24 h and the other for another 24 h, thereby reducing the power consumption of the system.

At the end of this system, each water sample is divided into two different outlet samples. The pure water sample, which is the ultrapure water that will be injected into tritium detector, and the rejection water, whose turbidity is even greater than the water sample before treatment because it contains all the particles that have been extracted from the ultrapure water sample.

With this ultrapure water system we can process up to  $0.850 \text{ m}^3/\text{h}$  with a single line operating or  $1.480 \text{ m}^3/\text{h}$  with both, greatly overestimating the requirements of the tritium detector.

The software used for remote controlling the ultrapure water system is Siemens PLC, with which we receive information fo this system such as the state of the valves, the pressure probes or water production in real time.

In the appendix D there are several photos showing each part of this system.

## 2.4 Background rejection system of TRITIUM monitor

The objective of this section is to reduce the radioactive background that affects the TRITIUM detector. It is important because we are following the ALARA principle for the tritium activity measurement, that is, to measure tritium activity "as low as reasonably achievable".

We have to take into account that the low limit reached in the tritium activity measured with our detector will be limited due to the uncertainty in the activity of the radioactive background measured since we cannot measure tritium activities lower than this uncertainty. Therefore, if we want to measure tritium activities as low as possible, we must reduce this background uncertainty as much as possible.

The total uncertainty of the measurement is a quadratic sum of all the different uncertainties present in this measurement, which is the statistical uncertainty,  $\sigma_{st}$ , (due to the statistical nature of the radioactivity process), the systematic uncertainty,  $\sigma_{si}$ , (due to the manufacture of the detectors), etc (equation 2.10).

With the background rejection system of TRITIUM monitor we try to minimize the statistical component. Because of the Poissonian nature of the process, the statistical component of the uncertainty corresponds to the square root of the measured activity,  $A_m$ , equation 2.10, so, if we want to reduce this component, we must minimize the radiological background that affects our detector as much as possible.

$$\sigma_T^2 = \sigma_{st}^2 + \sigma_{si}^2 + \dots; \quad \sigma_{st;bac} = \sqrt{A_{m;bac}} \quad (2.10)$$

The background that affects the tritium detector is due to natu-

ral radioactivity, which is present in all parts of the earth and it has two main origins. On the one hand, it can come from radioactive elements of the natural radioactive series, shown in table 2.4, which are the primordial radioactive elements, those that are present since the formation of the earth. On the other hand, it can come from natural radiation received from extraterrestrial sources, called cosmic radiation, composed of high-energy particles, mainly protons and  $\alpha$ , which, when they interact with the particles in the Earth's atmosphere, generate a shower of muons, photons and neutrons mainly.

Mass Num.	Series	Prim. el.	Half life (y)	Final isotope
4n	Thorium	$^{232}\text{Th}$	$1.41 \cdot 10^{10}$	$^{208}\text{Pb}$
4n+1	Neptunium	$^{237}\text{Np}$	$2.14 \cdot 10^6$	$^{209}\text{Pb}$
4n+2	Uranium-Radium	$^{238}\text{U}$	$4.51 \cdot 10^9$	$^{206}\text{Pb}$
4n+3	Uranium-Actinium	$^{235}\text{U}$	$7.18 \cdot 10^8$	$^{204}\text{Pb}$

Table 2.4: Classification of natural radioactive series [85][86].

Natural radioactivity depends on the altitude and latitude at which we are on Earth because the volume of the Earth's atmosphere, with which cosmic rays interact, is different. For the same reason, it also depends on the height at which we are working, at sea level in our case, and, due to the relative position of the earth in the universe, it also depend on the solar activity cycle in which we are when we measure. The spatial distribution of cosmic rays, mainly muons, follows a  $\cos^2(\theta)$  distribution with the zenith angle.

We will divide this natural radioactivity into two parts and we will use a different technique to prevent these events from affecting the tritium measurement:

- On the one hand, we have weak radiation, which is any radiation whose energy emission is below 200 MeV/nucleon. To avoid that these events

affect the tritium measurement, we will use a lead shield, explained in the section 2.4.1, with which we stop this radiation before it reaches the tritium detector.

- On the other hand, we have the hard radiation, that is, any radiation whose energy emission is greater than 200 MeV/nucleon (mainly cosmic radiation). We have to keep in mind that it is much more difficult to stop hard radiation than weak radiation, so instead of stopping this radiation, what we will do is to build an active veto, which are explained in the section 2.4.2, with which we only detect a hard cosmic event and it will be used in anti-coincidence with the TRITIUM detector, that is, we will save the measured tritium event just when we don't measure any hard cosmic event in time coincidence.

#### 2.4.1 Set up of the passive shield (lead)

To stop the weak radiation we use the so-called passive veto, which consists of a lead shielding inside which we will place the TRITIUM detector. This lead shielding is used to stop external particles before they reach the tritium detector, affecting the tritium measurement. It will work for particle energies below 200 MeV/nucleon, which is mainly the earth's natural radioactivity and the weak component of cosmic radiation.

This lead shielding consists of 158 lead bricks with ultra-low intrinsic radioactivity,  $A \approx NUMBER$ . The thickness of these bricks are 25 mm and they are shaped like a chevron, shown in the figure 2.23a, specially designed for a perfect fit and easy assembly. As can be seen in the figures 2.23b and 2.23c, these lead bricks are arranged in two layers leaving a total thickness of the lead shielding walls of 50 mm and the space between the lead bricks in the inner layer is overlaid with a lead brick of the outer layer to avoid possible entry of radiation.

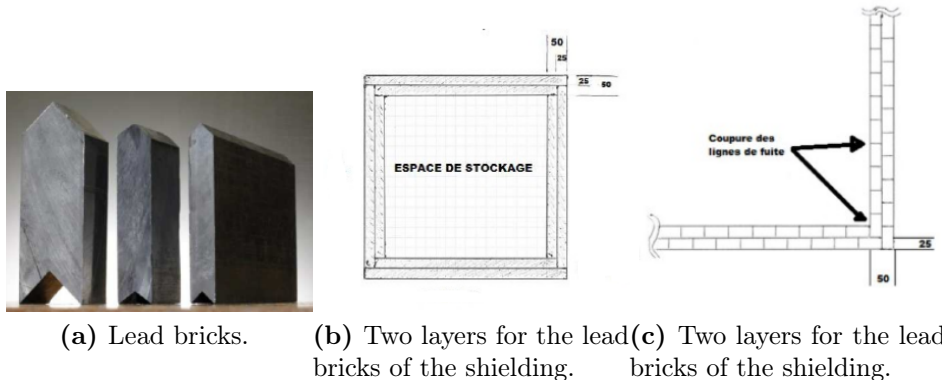


**Figura 2.23** – Lead Bricks and their arrangement in the lead shielding.

Mechanical engineering department of CENBG has designed a special aluminum structure, shown in figure 2.24, to support the total weight of the lead bricks, 2.4 tons.

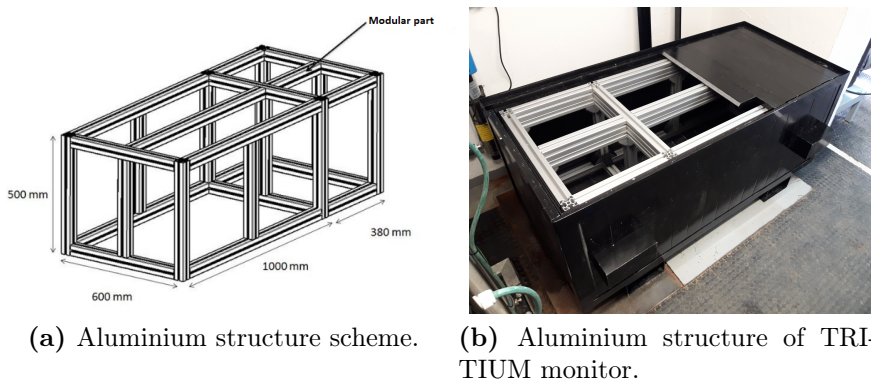


**Figura 2.24** – Lead Bricks and their arrangement in the lead shielding.

The internal space of this lead shielding is arranged in two parts, shown in figure 2.23. The one, larger, has an internal dimensions of 90.5 cm long, 41 cm deep, and 51 cm high and it will be used to place the TRITIUM detector. The other, smaller, has an internal dimensions of 33 cm long, 41 cm deep, and 51 cm high and it will serve to place the electronic system

necessary to collect and store data. The external dimensions of this lead shielding are 148 cm long, 60 cm deep and 70 cm high and a weight of 2.5 tons.

## 2.4.2 Set up of the active shield (cosmic veto)

For this section we have to take into account that the mean free path of particles is proportional to their energy. Therefore, we would need too thick walls to build a lead shield that would be able to stop hard radiation, mainly cosmic radiation. Instead of trying to stop it, we have used the so-called active vetos.

The active veto consists of several complementary detectors, called cosmic detectors, two complementary detectors for each active veto in our case, with which the hard cosmic events that affect the tritium measurement will be detected and subtracted from the tritium measurement.

As you can see in the figure 2.25, the way we have done it is to place two complementary detectors, one above the TRITIUM detector and the other below it.

We must keep in mind that we only want to eliminate the hard cosmic events that affect the tritium measurement. For that we must take into account that this active veto must be placed within the lead shielding. This is because, in this case, the weak radiation, which can contribute as a false hard comic events, has been removed.

Each cosmic detector will have two photosensors, four photosensors in each active veto. The most likely hard cosmic events that can affect the tritium measurement will pass through both cosmic detectors at the same time. To eliminate only them, the first thing we will do is detect only these hard cosmic events, which is achieved by reading both cosmic detectors in

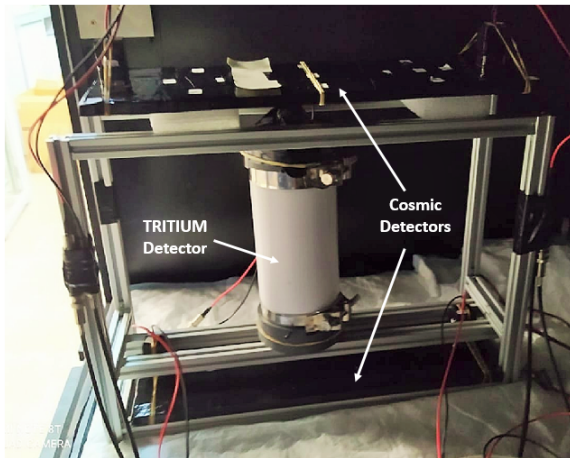


**Figura 2.25** – Active veto and Tritium-IFIC 2 prototype in an aluminum mechanical structure developed by IFIC's mechanical engineering department.

coincidence with the electron configuration shown in figure 2.16b and then we will read the TRITIUM detector in anti-coincidence with the active veto, that is, store the tritium measurement only when we don't detecte any hard cosmic event in the active veto in time coincidence.

In this case, if we have detect a hard cosmic event (time coincidence event in both cosmic detectors), we can be quite sure that it will cross through the tritium detector and, therefore, it will affect to their measurement, as you can see in the figure 2.26a.

There is a possibility that this hard cosmic event detected in the active veto comes from two different hard cosmic events (one detected in each cosmic detector as shown in figure 2.26b but it is practically negligible.

The number of hard cosmic events expected at sea level for muons, which is the main contributor of cosmic radiation at this height, is  $70 \text{ m}^{-2}\text{s}^{-1}\text{sr}^{-1}$  [87][88], that is, approximately,  $10^{-2} \text{ cm}^{-2}\text{s}^{-1}\text{sr}^{-1}$ , as you can see in their cosmic rate plot, shown in figure 2.26c. If we take into account that we are doing time coincidences with signals whose width is of the order of 10 ns we

can see that the probability of obtaining two different hard cosmic events in temporal coincidence is less than  $10^{-9}$  which is practically insignificant so they are not worth considering.

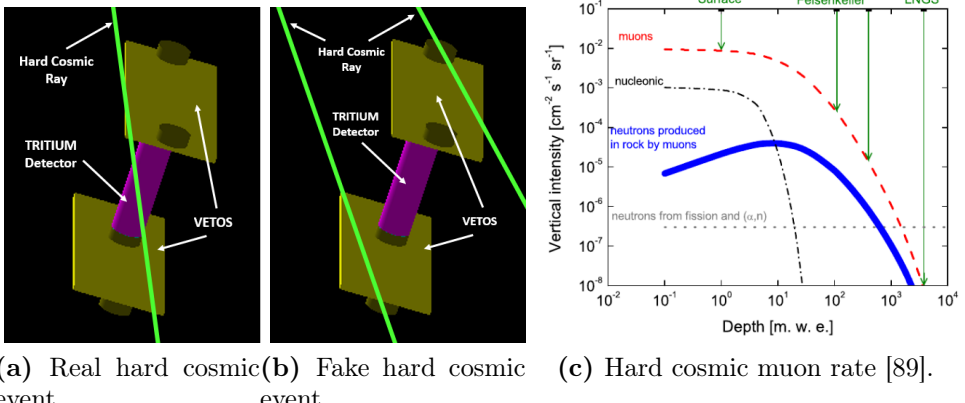


**Figura 2.26** – Hard cosmic events detected with the active veto of TRITIUM: a) Affecting to the tritium measurement, b) Does not affecting to the tritium measurement. c) Hard cosmic muon rate [89].

Finally, these individual cosmic detectors, on which the active veto is based, consist of a plastic scintillator block from Epic-Crystal [90], whose properties and energy emission spectrum are shown in table 2.5 and figure 2.27 respectively.

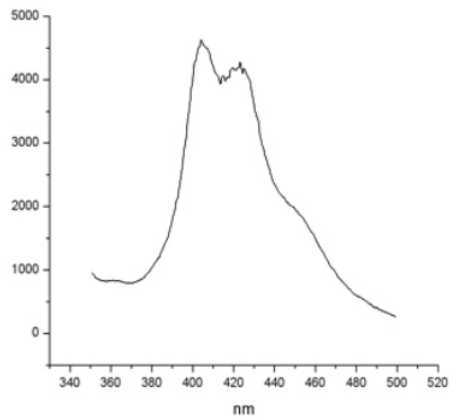
The dimensions used are 45 cm long, 17 cm deep and 1 cm of thickness and they are covered by three layers, teflon, aluminum and black tape, shown in figure 2.28, which is used, on the one hand, to prevent external photons from reaching the scintillator plastic, giving false hard cosmic events and, on the other hand, to prevent the photons generated by the scintillator plastic from escaping before reaching the photosensor, losing real hard cosmic events.

This coating has two  $2.5 \cdot 2.5 \text{ cm}^2$  windows where we can place both photosensors to read the photons produced by the plastic scintillator.

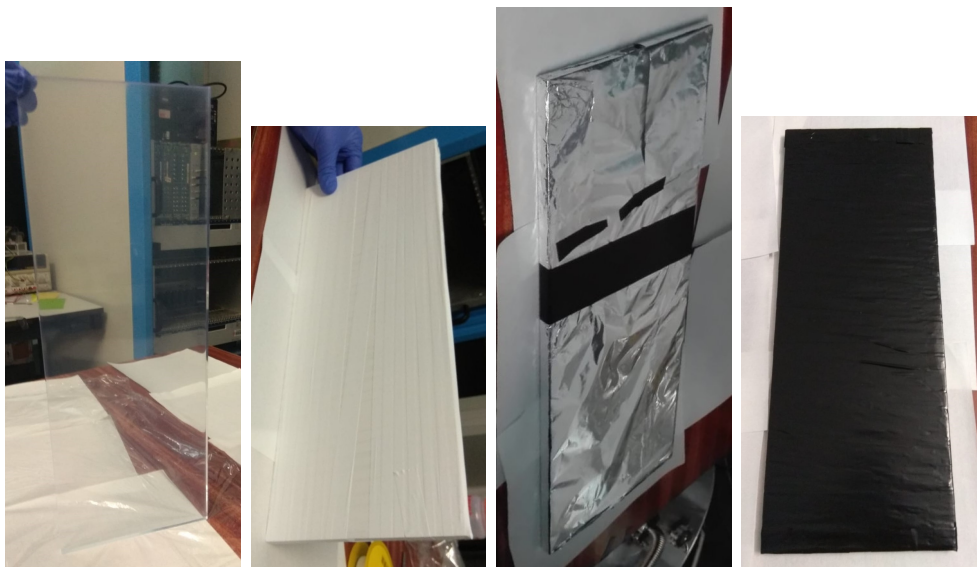
Base material	Polystyrene
Growth method	Polymeric
Density (g/cm <sup>3</sup> )	1.05
Refractive index	1.58
Soften temperature (°)	75-80
Light output (Anthracene)	50-60%
H/C raito	1.1
Emission peak (nm)	415 (Blue)
Decay Time, (ns)	2.4
Hygroscopic	No

Table 2.5: Properties of plastic scintillator blocks from Epic-Crystals. [90]

Now, we can calculate the expected hard cosmic rate for our specifically active vetos. As we have seen before, the expected hard cosmic rate at sea level is  $10^{-2} \text{ cm}^{-2}\text{s}^{-1}\text{sr}^{-1}$ . If we take into account that, on the one hand, the solid angle of our detectors is  $\omega = 0.5434$ , which has been calculated by integrating above the area of the TRITIUM active veto, and the area of its active veto is  $45 \text{ cm} \cdot 17 \text{ cm} = 765 \text{ cm}^2$ , the expected hard cosmic rate on our active vetos should be 2,909 event/s.



**Figura 2.27** – Emission energy spectrum of the plastic scintillation used for the active vetos. [90]



(a) Scintillator with- (b) Teflon coating. (c) Aluminium coat-(d) Black tape coat-out coating. ing. ing.

**Figura 2.28** – Different layers used to cover of the active veto.

# Chapter 3

## Research & Development on detector design and components

### 3.1 Introduction

This chapter shows the characterization of each individual part of the TRITIUM monitor, which includes scintillating fibers, SiPMs (at the individual SiPM level and at the matrix level), the ultrapure water system and the background rejection system, consisting of the lead shielding and the active veto.

This characterization is one of the most important things to do because it will help us to understand their behaviour and the results obtained with the complete monitor. Furthermore, we have made some developments to improve interesting parameters of the TRITIUM monitor components to enhance the monitor's capabilities for tritium detection.

All these studies have been carried out inside a special light-tight black box to ensure that the photons we are detecting come from the pho-

ton sources used, whether they are emitted by LEDs or by scintillators. Furthermore, because of the reason that we cannot do an accurate energy calibration when using plastic scintillators, we will show some energy spectrums in units of channels (units of ADC), which are linearly proportional to the units of energy.

## 3.2 Characterization and R&D on scintillating fibers

### Introduction

In this section we will try to measure experimentally the parameters of scintillating fibers that most affect the detection of tritium, such as their uncertainty in its preparation and conditioning process or the uncertain in its light collection efficiency.

We have to take into account that we are working with thousands of scintillating fibers that need to be prepared and conditioned prior to use in fiber studies or inside of TRITIUM monitor. Therefore, as we will see in this section, we had to develop machines to be able to prepare many fibers at the same time and automatically.

### Scintillating fiber conditioning process.

The first thing we had to do was choose the optimal fiber length at which the signal from the tritium events is optimized. To make this decision we have to take into account that, on the one hand, long fibers are interesting because the efficiency of our detector is proporcional to the active area, which is proporcional to the fiber length but, on the other hand, in long fibers, scintillation photons will need to be reflected in the fiber walls more times to be driven to its ends, where it will be detected by photosensors, and this is a problem because we lose photons in each reflection, deteriorating the detector signal.

Several simulations were performed using Geant4 [91], a particle and nuclear physics simulation package based on C++, to check the importance of this effect between other things and to allow us to choose the

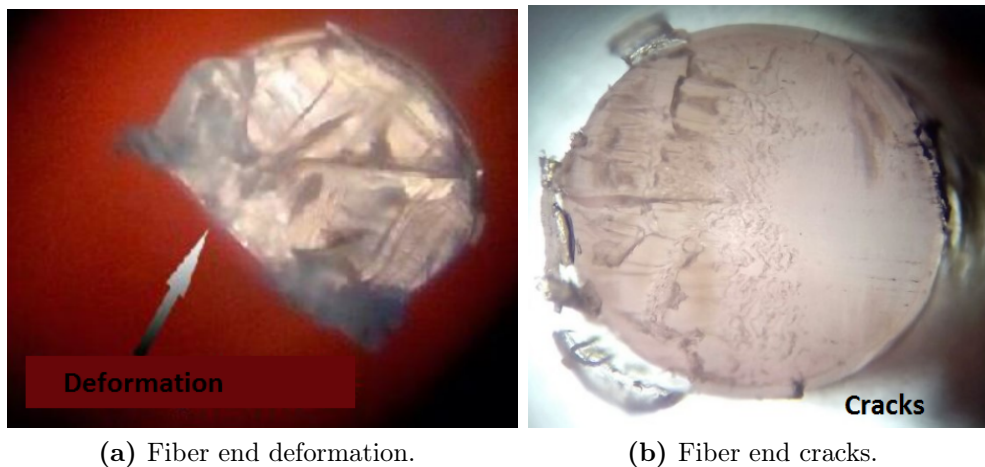
optimal fiber length. The results of this simulations will be shown in the section ?? where they will be discussed. In these simulations it has been seen that it is preferable to work with short fiber (figure ??). The fiber length, which has been chosen for the tritium prototypes developed in Valencia, is 20 cm and the fiber length used in each study will be named in the appropriate section, but it will be close to this value.

Saint Gobain's commercial fibers are 1 meter long, so first thing we had to do was cut the scintillation fibers before using it. It is very important to introduce strict requirements on the cutting quality of the fiber ends since it will greatly affect the transmission of photons and, thus, the efficiency of TRITIUM monitor. This cut must be perpendicular to the fiber and very low uncertainty in the length of the fiber to achieve a good coupling with the surface of the photosensor. It is also important that its final state must be as clean as possible, that is, without cracks or deformations because it will contribute to internal reflections, losing photons and, thus, reducing the tritium signal.

Cutting the end faces of polymer fibers is one of current challenges. There are many different techniques such as focused-ion-beam, milling, laser cutting, blade cutting, etc. Due to its simplicity, we have focused on blade cleaving.

Many commercial devices based on blade cleaving, such as the one provided by thorlabs with a diamond tipped blade [92] or the guillotine designed for industrial fiber optics [93], were tested in a extensive study done but with unsuccessful results [58]. As can be seen in the figures 3.1, it presents deformations, cracks or imperfections so the technics considered in this study don't overcome the requirements imposed.

A microscope model PB 4161 from EUROMEX company and the Digital Microscope from Jiusion company, shown in figures 3.2, were used to check the results in the fiber ends.



(a) Fiber end deformation.

(b) Fiber end cracks.

**Figura 3.1** – Unsuccessful results of using commercial techniques to cut fibers.

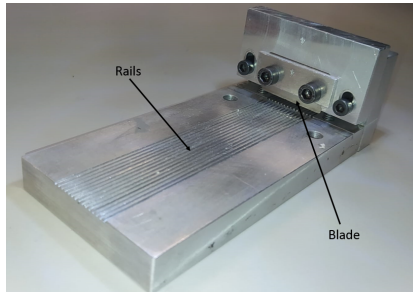


(a) EUROMEX microscope

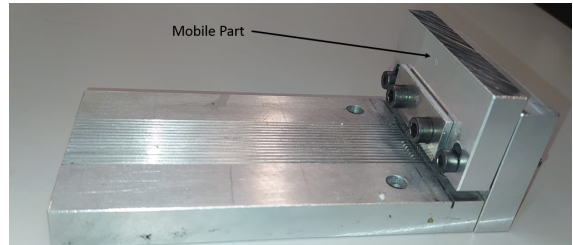
(b) Jiusion microscope

**Figura 3.2** – Microscopes used to check the results.

Because commercial devices don't work for our scintillating fibers, we had to design, build and test our own cutting device, which is shown in figure 3.3.



(a) TRITIUM Cutting device



(b) TRITIUM Cutting device



(c) Additional piece of TRITIUM cutting device

**Figura 3.3** – Cutting device developed in the TRITIUM experiment and additional part to make precise measurements of fiber length.

It consists of fourteen rails where the fibers will be fixed and a thin blade, fixed on a mobile piece perpendicular to the fibers, with which we can be sure of achieving a perpendicular cut, which is one of the requirements imposed.

The blade used is the typical commercial razor blade, whose thickness is 0.1 mm, which is the thickness with which we obtain the best results and it was positioned with a slight inclination, 5°, with respect to the horizontal axis since it has been seen in several studies that this helps to obtain a less aggressive and cleaner cut [94], [95].

Therefore, as can be seen in the figure 3.4a, with this device we ob-

tain fiber ends without breaks or deformation overcoming another imposed requirement.

Another important parameter that can affect the cutting quality of the ends of the fiber is the temperature of both, either the fiber or the blade. It has been tested in a study in which both were subjected to different temperatures from room temperature (25 degrees) to 110 degrees [58]. No significant conclusions were obtained in the temperature study, so we work at room temperature to facilitate the cutting technic.

To obtain a low enough length uncertainty, the last requirement we must overcome, we designed and built an additional piece, shown in figure 3.3c, which is used to measure the fiber. With this piece we achieve an uncertainty in the measurement of less than 1 millimeter.

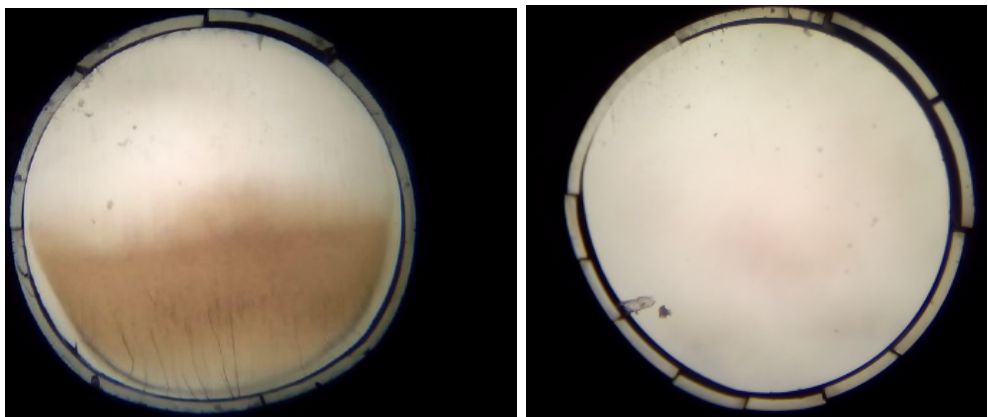
With the designed cutting fiber device we have exceeded all requirements imposed, obtaining a cut fiber end whose quality is high enough to ensure that it will affect the transmission of light as little as possible.

In the figure 3.4a you can see a slight darkening at the bottom of the fiber, which is an inevitable effect of the cutting process. To repair this imperfection, a polishing process developed by thorlabs is included [92].

This polishing process consists of using five different polishing papers, with a decreasing grain size, whose diameters are  $30 \mu\text{m}$ ,  $20 \mu\text{m}$ ,  $12 \mu\text{m}$ ,  $5 \mu\text{m}$  and  $0.3 \mu\text{m}$  respectively in which we describe movements in the shape of 8 for two minutes (approximately 120 movements).

The result obtained with this polishing process is shown in figure 3.4b. In the figure 3.4, the quality of both fiber ends, before and after polishing process, can be compared. There, we can see that the darkening has completely disappeared.

The end of the cut fiber is completely clear after cutting and pol-



(a) Fiber end after cutting with Tritium de-  
vice.  
(b) Fiber end after cutting and polish-  
ing.

**Figura 3.4** – Result of the polishing process. a) Fiber end after cutting with TRITIUM devices b) Fiber end after cutting with TRITIUM devices and polishing with Thorlabs technic.

ishing, without any damage or imperfection, so both tasks, cutting and polishing, will make up the conditioning process developed for each fiber before any study or introduction into the TRITIUM monitor.

### Characterization of Scintillating fibers

#### Polishing machine for scintillating fibers

#### Cleaning Process for scintillating fibers

### 3.3 Characterization and R&D on SiPM

Trabajo de Fernando Hueso.

Explicar electrónica que se utiliza como la tarjeta y demás. Poner el esquema electrónico de la tarjeta y referencia a Marc de NEXT por haberla construido. Explicar la forma del pulso como en la tesis de Katerina Asnar

Paper de Nadia para la PDE.

Las medidas se han hecho en la cámara del IFIMED (ver lo que tengo apuntado en el TFM y dar gracias al IFIMED)

la banda prohibida es pequeña por lo que algunos electrones pueden excitarse térmicamente y pasar a la banda de conducción -> RUIDO Cuando hable del ruido, afterpulses, crosstalk... intro en MPPC hammatsu data sheet

cuando hable de la capacidad del SiPM utilizar el punto 10.3.2 del Leo -> pag. 226

resumen de como varía cada magnitud con la temperatura y el voltaje. Tesis SiPMs.

Incoherent light source!

fired cells.

paper NADIA

B. Photon Detection Efficiency -> entero.

Aunque el aumentar el voltaje inverso mejora la eficiencia de detección de fotones, también aumenta la corriente oscura. Reducir la tem-

peratura sin embargo disminuye la corriente oscura.

Para contar el número de veces que dos o más fotones son detectados simultáneamente, el umbral les establecido en  $N - 0.5$  p.e. (donde  $N$  es un número arbitrario de fotones). Al contar el número de pulsos que exceden este umbral se puede saber el número de veces que se han detectado simultáneamente  $N$  o más fotones (Manual Hamamatsu, 2008, 2007)

En este trabajo se estudió tanto la variación en la resolución en energía de un SiPM como la variación del centroide de un pico (explicado a detalle en los próximos capítulos) con la temperatura y el voltaje. Para ello se estableció una electrónica de adquisición adecuada para la mayor eliminación de ruido posible y óptima resolución (explicada en el Capítulo 3).

Superponer 2 plots con el LED a distintos voltajes (2 o mas... probar varios voltajes a Vov recomendado y quedarnos con los mejores).

Figura 11 de la tesis de cristales monolíticos

La ganancia  $M$ , depende exponencialmente de la tensión de polarización inversa del dispositivo (Fig. 11, derecha). Sin embargo, en la región de operación de los APDs con  $M \approx 100$ , un cambio relativo de tensión de polarización corresponde a un cambio lineal en la ganancia, con pendientes típicas de 10 %/V. Además, la temperatura debe estar debidamente estabilizada en un sistema con APDs ya que estos detectores sufren variaciones importantes con la temperatura, típicamente 2-3 %/ °C

Todo el apartado de SiPMs de esta tesis.

Cuando hablamos del PDE: El número de celdas de un SiPM dependerá de la aplicación específica. Será lo suficientemente elevado para detectar la cantidad de fotones esperada pero sin exceder innecesariamente este valor, ya que cada celda necesita de espacio para las resistencias de

quenching de cada APD y para la separación y aislamiento entre las diferentes celdas. Cuanto mayor sea el número de celdas, mayor será el espacio muerto y menor su eficiencia. Por el contrario, un número de celdas inferior con celdas de mayor tamaño, implica una alta eficiencia de detección de fotones (Photon Detection efficiency, PDE) pero un rango dinámico bajo. La PDE en un SiPM se define como su eficiencia cuántica por el ratio entre el área sensitiva y el área total del dispositivo, lo que se conoce como factor de llenado (fill factor) y se representa con “epsilon”, por la probabilidad de que un fotoelectrón comience un proceso de avalancha (Ec. 19). Aparte de la longitud de onda,

Este parrafo justifica porque me quedo con el SiPM array de area de SiPM mayor... debido a la sensibilidad... punto 4.2 de la tesis de SiPM (LARGA)

the noise level scales with the area of the device.

If each ionization process could be considered independent of the others, the fluctuations would then be described by a Poisson distribution where the variance ( $\sigma^2$ ) would be equal to the mean number of ionization electrons,  $N_I$ . However, the fluctuations in the mean number of ionization electrons present a lower value, as predicted by Fano's theory [66], being proportional to a factor  $F$ , known as the Fano Factor, which multiplies the mean primary ionization yield.

Tiene un factor de amplificación interno que depende exclusivamente de las características de la unión p-n y de la resistencia quenching

### **3.4 Characterization and R&D on ultrapure water system**

Mostrar los datos del agua del río Tajo antes del sistema de purificación del agua (valores de conductividad, constituyentes químicos, etc) Diapositiva de José Ángel.

Mostrar también un espectro energético donde se identifiquen los isótopos radioactivos presentes en el agua antes del sistema.

Mostrar estos mismos datos después del sistema de purificación del agua.

En el espectro energético deberíamos ver muchos elementos presentes, incluido el tritio, que desaparecen en la muestra final. El nivel del tritio permanece.

Llegamos al nivel de pureza del agua adecuado? Esto daña las fibras? Se reduce la actividad de tritio?

Cantidad de agua que se puede llegar a procesar con el sistema.

## 3.5 Characterization and R&D on background shields

### 3.5.1 Passive shield (lead)

### 3.5.2 Active shield (cosmic veto)

Primero mostrar el espectro energético de antes y despues de recubrir el veto

A continuación mostrar los plateaus de HV y Thresholds.

Mostrar estudio para las dos posibles localizaciones de las ventanas en el VETO. Ligera mejora para la elegida.

Luego mostrar el mapeo realizado sobre el veto, tanto a nivel individual (hecha por Ana -> Coger las del voto S, que aunque salgan ligeramente diferentes si ) como a nivel coincidencia entre vetos.

Presentar la relación cuentas/segundo frente a distancia entre vetos y comparar con los datos calculados por computación numérica.

En este último incluir los datos para nuestra medida concreta, 36cm para PMTs y 32cm para SiPMs.

EFICIENCIA DE DETECCIÓN?? -> 85%

Ajustar a landau



# Chapter 4

## Tritium monitor prototypes

### 4.1 Preliminary prototypes, TRITIUM-IFIC 0, TRITIUM-IFIC 1 and TRITIUM-Aveiro

#### 4.1.1 Tritium-IFIC 0

#### 4.1.2 Tritium-IFIC 1

#### 4.1.3 Tritium-Aveiro

## **4.2 Advanced prototype, Tritium-IFIC 2**

## 4.3 Modular TRITIUM prototype for in-situ tritium monitoring

Hablar del esquema electrónico total. Muchos módulos y muchos vetos, etc...



# Chapter 5

## Simulations



# Chapter 6

## TRITIUM Monitor results and discussion

### 6.1 Results from laboratory measurements

## **6.2 Results from measurements at Arrocampo dam**

## 6.3 Results in simulations



# Chapter 7

## Conclusions and prospects

Que cosas se han conseguido en este experimento? -> DECIR que tanto lo que se ha conseguido con el detector como con las investigaciones de componentes del detector (capítulo 3)

Responder a las grandes preguntas:

- Podemos medir tritio?
- Lo podemos hacer en tiempo quasi real?
- Lo podemos hacer a la actividad que queríamos?
- Que sensibilidad se ha llegado a conseguir?
- Estabilidad temporal?
- Precio?
- Comparación con respecto al resto de experimentos? -> Poner la tabla 1.8 pero incluyéndonos
- Efecto del shield

- Efecto de los vetos
- Efecto de ambas cosas
- Medidas a varias actividades

Tenemos datos de tritio en el agua bruta (agua del río) de esa zona desde 1998, pero tengo que solicitar permiso para poder dártelos. En cualquier caso, hay otra manera de conseguirlos, que es a partir de los informes del CSN al Congreso de los diputados (web CSN). Desde 2015 la concentración de tritio en el agua del río Tajo ha disminuido considerablemente porque la CNA instaló unos enfriadores por convección que emiten parte del H3 a la atmósfera. -> Tesis de Antonio Rodríguez y de Elena García.

# Appendices



# Appendix A

## Birks coefficient study

Aún faltan cosas por decir.



## Appendix B

# Signal processing in NIM modules

Y más cosas aún.



## Appendix C

# Electronical schemes of PCBs used for SiPM characterization

Y más cosas aún.



# Appendix D

## Ultrapure water system

In this appendix I show several photos of the ultrapure water system in the same order that the water flows through them.

First of all, the complete scheme of the ultrapure water system is shown in figure D.1:

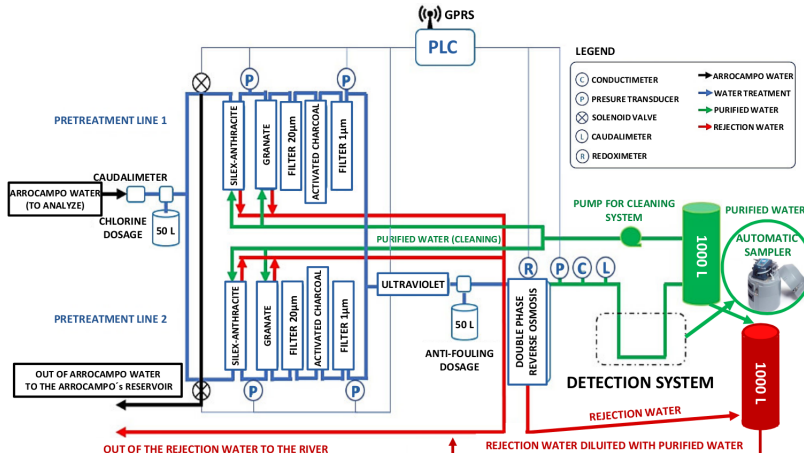


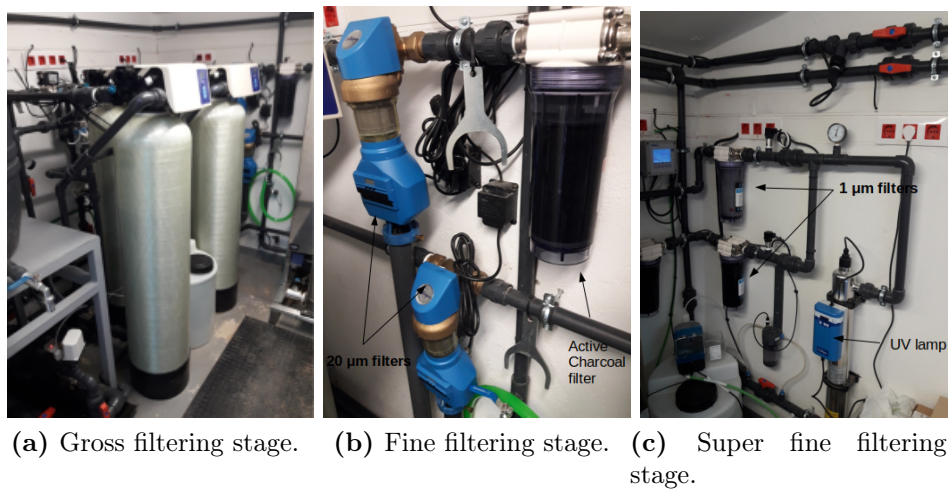
**Figura D.1** – Scheme of the ultrapure water system.

Secondly, the Gross filtering stage, made up of Silex-Antracite and

Granate filters, is shown in the figure D.2a:

In third place, the fine filtering stage, consisting of  $20\ \mu\text{m}$  filter and active carbon filter, is shown in figure D.2b:

In fourth place, the superfine filtering, composed of the  $1\ \mu\text{m}$  filter and the UV lamps, is shown in the figure D.2c



(a) Gross filtering stage. (b) Fine filtering stage. (c) Super fine filtering stage.

**Figura D.2** – Different stages of filtration of the ultrapure water system.

In fifth place, the double phase reverse osmosis is shown in figure D.3a

In sixth place, the containers in which we store the ultrapure water and the reject water after treatment is shown in figure D.3b.

In seventh place, the Siemens PLC, software used to control the ultrapure water system, is shown in figure D.4.

Finally, the complete system of the ultrapure water system is shown in the figure D.5

Just as a curiosity, the three types of water (raw water, rejection



(a) Doble phase reverse osmosis stage and (b) Storage containers of reject and ultrapure water.

**Figura D.3** – Doble phase reverse osmosis stage and containers used to store the outlet water of the ultrapure water system.

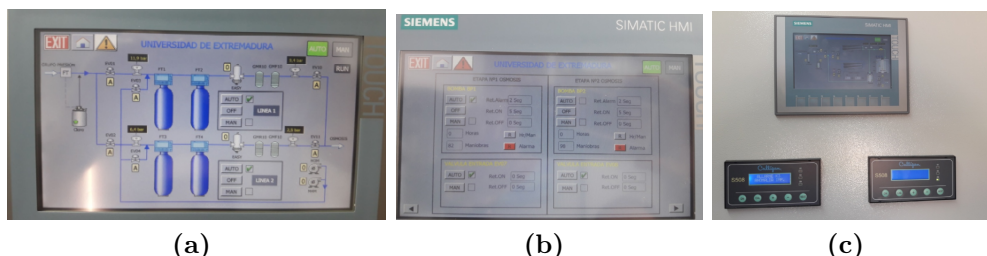


**Figura D.4** – Siemens PLC, software for remote control of ultrapure water system.



**Figura D.5** – General photo of the complete ultrapure water system.

water and ultrapure water) are shown in figure D.6, where you can visually check the difference in the turbidity of each type of water.

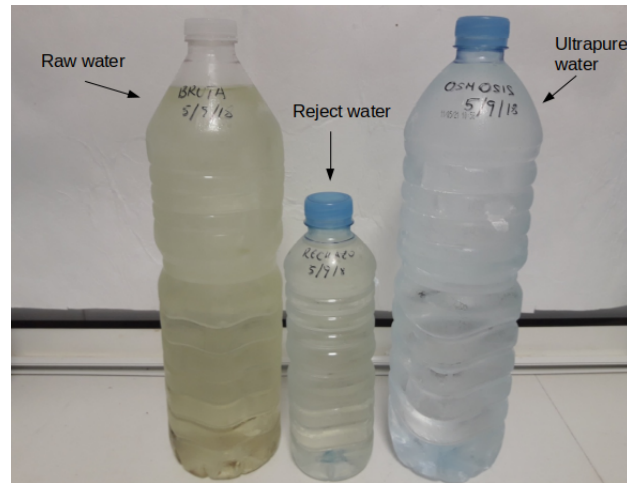


**Figura D.6** – Raw water, reject water and ultrapure water obtained with this system.

# Bibliography

- [1] F. J. ECHARTE, *El futuro de las energías renovables en España*, Universidad de Navarra. **TECNUN'01 IESE'13.**
- [2] *International Energy Outlook 2013*. U. E. Energy Information Administration.
- [3] UN news, *Global perspective Human stories*.
- [4] *Kyoto protocol and reference manual*, 2008, United Nations.
- [5] **ITER**, International Thermonuclear Experimental Reactor.
- [6] A. FIEGE, *Tritium*, Kernforschungszentrum Karlsruhe, 1992.
- [7] EDUARDO OLIVA GONZALO, ADRIANA ORTIZ GÓMEZ, NURIA MORAL FERNÁNDEZ, ALEJANDRO CARRASCO SÁNCHEZ, JOSÉ MANUEL PERLADO MARTÍN, RAQUEL SUÁREZ HONTORIA, MANUEL COTELO FERREIRO *Curso Básico de Fusión Nuclear*, jóvenes nucleares, Sociedad Nuclear Española, Septiembre de 2017, Madrid, Spain.
- [8] BENJAMIN K. SOVACOOL, *Valuing the greenhouse gas emissions from nuclear power: A critical survey*, ELSEVIER, Energy Policy Vol 36 p. 2940-2953. DOI:10.1016/j.enpol.2008.04.017

- [9] *Avance del informe del sistema eléctrico español, 2019, Red eléctrica española.*
- [10] *Three mile island accident, World Nuclear Association.*
- [11] *Cierre de centrales nucleares en España antes de 2030, Cinco Días, El País.*
- [12] *China construirá 60 centrales nucleares en la próxima década, Europa press.*
- [13] *Inversión de EE. UU. de 35 millones para centrales nucleares, Energy News.*
- [14] J. W. BERTHOLD, L. A. JEFFERS, *Phase 1 Final Report for In-Situ Tritium Beta Detector*, U. S. Department of Energy, McDermott Technology, Inc., Research and Development Division, **DE-AC21-96MC33128**, April, 1998.
- [15] J. W. BERTHOLD, L. A. JEFFERS, *In Situ Tritium Beta Detector*, U. S. Department of Energy, McDermott Technology, Inc. (MTI), Technology development data sheet, **DE-AC21-96MC33128**, May, 1999.
- [16] X- HOU, *Tritium and  $^{14}C$  in the environmental and nuclear facilities: Sources and analytical methods*, Journal of the Nuclear Fuel Cycle and Waste Technology (JNFCWT), 16 (2018), 11-39 **DOI: 10.7733/jnfcwt.2018.16.1.11.**
- [17] Tritium at Fermilab.
- [18] **Brookhaven National Laboratory (BNL).**
- [19] ALEKSANDRA SAWODNI, ANNA PAZDUR, JACEK PAWLICZAK, *Measurements of Tritium Radioactivity in Surface Water on the Upper Silesia Region*, Journal on Methods and Applications of Absolute Chronology, Geochronometria, Vol. 18, pp 23-28 **2000.**

- [20] *Council directive 2013/15/euratom.*
- [21] TITLE 40, *Protection of the Environment, US Code of Federal Regulations* Part 141, Section 66, June 2011, **e-CFR (Electronic Code of Federal Regulations)**.
- [22] *REFERENCIAAAAAAAA*.
- [23] M. L. OLIPHANT, P. HARTECK and E. RUTHERFORD, *Transmutation Effects observed with Heavy Hydrogen*, Nature, 133, 413 (1934) **DOI: 10.1038/133413a0**.
- [24] LUIS W. ALVAREZ and R. CORNOG, *Helium and Hydrogen of Mass 3*, Physical Review Journals Archive, 53, 613 (1939) **DOI: 10.1103/PhysRev.56.613**.
- [25] *DOE Handbook: Primer on Tritium Safe Handling Practices*, U. S. Departament Of Energy Washington, D.C. 20585.
- [26] ROBERT HAIGHT, JOSEPH WERMER and MICHAEL FIKANI, *Tritium Production by Fast Neutrons on Oxygen: An Integral Experiment*, Journal of Nuclear Science and Technology, 39:sup2, 1232-1235, **DOI: 10.1080/00223131.2002.10875326**.
- [27] , *REFERENCIAAAAA*,
- [28] *International Atomic Energy Agency*.
- [29] *Tritium decay image*.
- [30] ZOLTÁN KÖLLO, *Tesis: Studies on a plastic scintillator detector for activity measurement of tritiated water*, Facultad de Física, Instituto Tecnológico de Karlsruhe (KIT), Karlsruhe, Alemania, 17/07/2015, **DOI: 10.5445/IR/1000049424**
- [31] SYLVER HEINZE, THIBAUT STOLZ, DIDIER DUCRET and JEAN-CLAUDE COLSON, *Self-Radiolysis of Tritiated Water: Experimental*

*Study and Simulation*, Fusion Science and Technology, 48:1, 673-679,  
**DOI: 10.13182/FST05-A1014**

- [32] , , and , , , ,
- [33] M. N. AL-HADDAD, A. H. FAYOUMI and F. A. ABU-JARAD, *Calibration of a liquid scintillation counter to assess tritium levels in various samples*, Nuclear Instruments and Methods in Physics Research A, Volume 438, Issues 2-3, December 1999, Pages 356-361, **DOI: 10.1016/S0168-9002(99)00272-7**.
- [34] K. J. HOFSTETTER and H. T. WILSON, *Aqueous Effluent Tritium Monitor Development*, Fusion Technology, Volume 21, 2P2, Pages 446-451, March 1992, **DOI: 10.13182/FST92-A29786**.
- [35] M. PALOMO. A. PEÑALVER, C. AGUILAR and F. BORRULL, *Tritium activity levels in environmental water samples from different origins*, Applied Radiation and Isotopes, Volume 65, Issue 9, September 2007, Pages 1048-1056, **DOI: 10.1016/j.apradiso.2007.03.013**.
- [36] R. A. SIGG, J. E. McCARTY, R. R. LIVINGSTON and M. A. SANDERS, *Real-time aqueous tritium monitor using liquid scintillation counting*, Nuclear Instrument and Methods in Physics Research A, Volume 353, Issues 1-3, 30 Decembre 1994, Pages 494-498 **DOI: 10.1016/0168-9002(94)91707-8**.
- [37] N. P. KHERANI, *An alternative approach to tritium-in-water monitoring*, Nuclear and Methods in Physics Research A, Volume 484, Issues 1-3, 21 May 2002, Pages 650-659 **DOI: 10.1016/S0168-9002(01)02008-3**
- [38] Z. CHEN, S. PENG, D. MENG Y. HE and H. WANG, *Theoretical study of energy deposition in ionization chambers for tritium measurements*, Review of Scientific Instruments, 84, 103302, 2013, **DOI: 10.1063/1.4825032**.

- [39] C. G. ALECU, U. BESSERER, B. BORNSCHEIN, B. KLOPPE, Z. KÖLLÖ and J. WENDEL, *Reachable Accuracy and Precision for Tritium Measurements by Calorimetry at TLK*, Fusion Science and Technology, 60:3, 937-940, DOI: [10.13182/FST11-A12569](https://doi.org/10.13182/FST11-A12569).
- [40] A. BÜKKI-DEME, C. G. ALECU, B. KLOPPE and B. BORNSCHEIN, *First results with the upgraded TLK tritium calorimeter IGC-V0.5*, Fusion Engineering and Design, Volume 88, Issue 11, November 2013, Pages 2865-2869 DOI: [10.1016/j.fusengdes.2013.05.066](https://doi.org/10.1016/j.fusengdes.2013.05.066).
- [41] M. MATSUYAMA, Y. TORIKAI, M. HARA and K. WATANABE, *New Technique for non-destructive measurements of tritium in future fusion reactors*, IAEA Nuclear Fusion, Volume 47, Number 7, S464, June 2007, DOI: [10.1088/0029-5515/47/7/S09](https://doi.org/10.1088/0029-5515/47/7/S09).
- [42] M. MATSUYAMA, *Development of a new detection system for monitoring high-level tritiated water*, Fusion Engineering and Design, Volume 83, Issue 10-12, December 2008, Pages 1438-1441 DOI: [10.1016/j.fusengdes.2008.05.023](https://doi.org/10.1016/j.fusengdes.2008.05.023).
- [43] S. NIEMES, M. STURM, R. MICHLING and B. BORNSCHEIN, *High Level Tritiated Water Monitoring by Bremsstrahlung Counting Using a Silicon Dift Detector*, Fusion Science and Technology, 67:3, 507-510, 2015, DOI: [10.13182/FST14-T66](https://doi.org/10.13182/FST14-T66).
- [44] K. S. SHAH, P. GOTHSKAR, R. FARRELL and J. GORDON, *High Efficiency Detection of Tritium Using Silicon Avalanche Photodiodes*, IEEE Transactions on Nuclear Science, Volume 44, Issue 3, June 1997, DOI: [10.1109/23.603750](https://doi.org/10.1109/23.603750)
- [45] P. JEAN-BAPTISTE, E. FOURRÉ, A. DAPOIGNY, D. BAUMIER, N. BAGLAN and G. ALANIC,  *$^3\text{He}$  mass spectrometry for very low-level measurement of organic tritium in environmental samples*, Journal of Environmental Radioactivity,

- Volume 101, Issue 2, February 2010, Pages 185-190, DOI: <https://doi.org/10.1016/j.jenvrad.2009.10.005>.
- [46] C. BRAY, A. PAILOUX and S. PLUMERI, *Tritiated water detection in the 2.17  $\mu\text{M}$  spectral region by cavity ring down spectroscopy*, Nuclear Instruments and Methods in Physics Research A, Volume 789, 21 July 2015, Pages 43-49, DOI: [10.1016/j.nima.2015.03.064](https://doi.org/10.1016/j.nima.2015.03.064).
  - [47] M. MURAMATSU, A. KOYANO and N. TOKANUGA, *A Scintillation Probe for Continuous Monitoring of Tritiated Water*, Nuclear Instruments and Methods, Volume 54, Issue 2, October 1967, Page 325-326, DOI: [10.1016/0029-554X\(67\)90645-3](https://doi.org/10.1016/0029-554X(67)90645-3).
  - [48] A. A. MOGHISSI, H. L. KELLEY, C. R. PHILLIPS and J. E. REGNIER, *A Tritium Monitor Based on Scintillation*, Nuclear Instruments and Methods, Volume 68, Issue 1, 1 February 1969, Page 159, DOI: [10.1016/0029-554X\(69\)90705-8](https://doi.org/10.1016/0029-554X(69)90705-8).
  - [49] R. V. OSBORNE, *Detector for Tritium in Water*, Nuclear Instruments and Methods, Volume 77, Issue 1, 1 January 1970, Page 170-172, DOI: [10.1016/0029-554X\(70\)90596-3](https://doi.org/10.1016/0029-554X(70)90596-3).
  - [50] A. N. SINGH, M. RATNAKARAN and K. G. VOHRA, *An Online Tritium-in-Water Monitor*, Nuclear Instruments and Methods, Volume 236, Issue 1, 1 May 1985, Page 159-164, DOI: [10.1016/0168-9002\(85\)90141-X](https://doi.org/10.1016/0168-9002(85)90141-X).
  - [51] M. RATNAKARAN, R. M. REVETKAR, R. K. SAMANT and M. C. ABANI, *A Real-time Tritium-In-Water Monitor for Measurement Of Heavy Water Leak To The Secondary Coolant*, International congress of the International Radiation Protection Association, Volume 32, Issue 15, 14-19 May 2000, P-3a-197, Reference number: **32015986**
  - [52] K. J. HOFSTETTER and H. T. WILSON, *Aqueous Effluent Tritium Monitor Development*, Fusion Technology, Volume 21, 2P2, 1992, Pages 446-451, DOI: [10.13182/FST92-A29786](https://doi.org/10.13182/FST92-A29786).

- [53] K. J. HOFSTETTER and H. T. WILSON, *Continuous Tritium Effluent Water Monitor at the Savannah River Site*, International conference on advances in liquid scintillation, Vienna (Austria), 14-18 September 1992.
- [54] *Tritium, Interreg Sudoe Program. Tritium website.*
- [55] GLENN F. KNOLL, *Radiation Detection and Measurement*, Third Edition, John Wiley and Sons, Inc. 1999.
- [56] WILLIAM R. LEO, *Techniques for Nuclear and Particle Physics Experiments: a how-to approach*, Second Revised Edition, Springer-Verlag Berlin Heidelberg GmbH, 1994. DOI: **10.1007/978-3-642-57920-2**.
- [57] SAINT-GOBAIN CERAMICS AND PLASTICS, INC., *Organic Scintillation Materials and Assamblies*, It's What's Inside that Counts, 2001-20. **Data sheet**.
- [58] , , .
- [59] *Plastic Scintillating Fibers*, Scintillating Fibers, Wavelength Shifting Fibers and Clear Fibers. **Data sheet**.
- [60] , , .
- [61] JAVIER PÉREZ PÉREZ, *Caracterización de los Fotomultiplicadores R8520-06SEL para NEXT*, 25-06-2010.
- [62] HAMMAMATSU PHOTONICS K.K., *Photonmultiplier tube R8520-406/R8520-506*. **Data sheet**.
- [63] DAVID LORCA GALINDO, *Tesis: SiPM based tracking for detector calibration in NEXT*, Departamento de física atómica, molecular y nuclear, Universidad de Valencia (UV), Valencia, Spain, 03/2015.
- [64] OSI OPTOELECTRONICS, *Characteristics and Applications*.

- [65] HAMMAMATSU PHOTONICS K.K. SOLID STATE DIVISION, *MPPC Multi-Pixel Photon Counter S13360-6050*. **Data sheet**.
- [66] HAMMAMATSU PHOTONICS K.K. SOLID STATE DIVISION, *MPPC Multi-Pixel Photon Counter S13360-6075*. **Data sheet**.
- [67] HAMMAMATSU PHOTONICS K.K. SOLID STATE DIVISION, *MPPC Multi-Pixel Photon Counter S13361-6050*. **Data sheet**.
- [68] HAMMAMATSU PHOTONICS K.K. SOLID STATE DIVISION, *MPPC Multi-Pixel Photon Counter S13361-3050*. **Data sheet**.
- [69] SENSL SENSE LIGHT, *Introduction to the SPM TECHNICAL NOTE*. February 2017 **Document**.
- [70] KEITHLEY, A GREATER MEASURE OF CONFIDENCE, *Model 6487 Picoammeter/voltage source, Manual reference*. **Data sheet**.
- [71] TENNELEC, *Model TC 952 High Voltage Supply, Manual reference*. **Data sheet**.
- [72] WENZEL ELECTRONIK, *Model N 1330-4 High Voltage Power Supply*. **Website**.
- [73] PHILIPS SCIENTIFIC, *Model 740 Quad Linear Fan-In/Out, Manual reference*. **Data sheet**.
- [74] ORTEC, *Model 9326 FastPreamplifier, Manual reference*. **Data sheet**.
- [75] ORTEC, *Model 575A Amplifier, Manual reference*. **Data sheet**.
- [76] ORTEC, *Model 671 Spectroscopy Amplifier, Manual reference*. **Data sheet**.
- [77] ORTEC, *Model CF8000 Octal Constant-Fraction Discriminator, Manual reference*. **Data sheet**.

- [78] CAEN, *Model 84, 4 channels discriminator*. **Website**.
- [79] LECROY, *Model 465 Coincidence Unit, Manual reference*. **Data sheet**.
- [80] ORTEC, *Model 416A Gate and Delay Generator, Manual reference*. **Data sheet**.
- [81] AMPTEK, *MCA8000D, Pocket MCA, Digital Multichannel Analyzer, Manual reference*. **Data sheet**.
- [82] PETsys Electronics. **Website**.
- [83] SAINT GOBAIN, *Optical fiber BCF-98, Manual reference*. **Manual reference**.
- [84] , .
- [85] PALL THEODÓRSSON, *Measurement of weak radioactivity*, World Scientific, 1996.
- [86] R D EVANS, *The Atomic Nucleus*, McGraw-Hill, Inc., 1996.
- [87] P.A. ZYLA ET AL., (*Particle Data Grup*), *PDG, Prog. Theor. Exp. Phys.* **2020** no. 8, 083C01 (2020). **Website DOI:** [10.1093/ptep/ptaa104](https://doi.org/10.1093/ptep/ptaa104).
- [88] HIROYUKI SAGAWA & ITSUMASA URABE (2001), *Estimation of Absorbed Dose Rates in Air Based on Flux Densities of Cosmic Ray Muons and Electrons on the Ground Level in Japan*, *Journal of Nuclear Science and Technology*, 38:12, 1103-1108, **DOI:** [10.1080/18811248.2001.9715142](https://doi.org/10.1080/18811248.2001.9715142).
- [89] T. SZÜCS, D. BEMMERER, T. P. REINHARDT, K. SCHMIDT, M. P TAKÁCS, A. WAGNER, L. WAGNER, D. WEINBERGER AND K. ZUBER, *Cosmic-ray induced background intercomparison with actively shielded HPGe detectors at underground locations*. **DOI:** [10.1140/epja/i2015-15033-0](https://doi.org/10.1140/epja/i2015-15033-0).

- [90] EPIC CRYSTAL, *Plastic scintillator of Epic Crystal, Manual reference. Data sheet.*
- [91] GEANT4, *Geant4: A toolkit for the simulation of the passage of particles through matter.. Website.*
- [92] THORLABS, *Guide to connectorization and polishing optical fibers,* 2006. **Manual Reference.**
- [93] INDISTROÑ FIBER OPTICAL, *POF Cutter block.* **Website.**
- [94] DAVID SÁEZ-RODRÍGUEZ, KRISTIAN NIELSEN, OLE BANG AND DAVID JOHN WEBB, *Simple Room Temperature Method for Polymer Optical Fibre Cleaving,* Journal of lightwave technology, vol 33, No. 23, December 1, 2015. **DOI:10.1109/JLT.2015.2479365.**
- [95] S.H. LAW, J.D. HARVEY, R.J. KRUHLAK, M. SONG, E. WU, G.W. BARTON, M.A. VAN EIJKELNBORG AND M.C.J. LARGE, *Cleaving of microstructured polymer optical fibres.* **DOI:10.1016/j.optcom.2005.08.011.**